Journal of Neuroinflammation

RESEARCH Open Access

Up-regulated succinylation modifications induce a senescence phenotype in microglia by altering mitochondrial energy metabolism

Xinnan Zhao[1], Xiaohan Yang[1,2], Cong Du[1], Huimin Hao[1], Shuang Liu[1], Gang Liu[1], Guangyin Zhang[1], Kai Fan[1] and Jianmei Ma[1,3*]

Abstract

The aging of the central nervous system(CNS) is a primary contributor to neurodegenerative diseases in older individuals and significantly impacts their quality of life. Neuroinflammation, characterized by activation of microglia(MG) and release of cytokines, is closely associated with the onset of these neurodegenerative diseases. The activated status of MG is modulated by specifically programmed metabolic changes under various conditions. Succinylation, a novel post-translational modification(PTM) mainly involved in regulating mitochondrial energy metabolism pathways, remains unknown in its role in MG activation and aging. In the present study, we found that succinylation levels were significantly increased both during aging and upon lipopolysaccharide-induced(LPS-induced) MG activation undergoing metabolic reprogramming. Up-regulated succinylation induced by sirtuin 5 knockdown(Sirt5 KD) in microglial cell line BV2 resulted in significant up-regulation of aging-related genes, accompanied by impaired mitochondrial adaptability and a shift towards glycolysis as a major metabolic pathway. Furthermore, after LPS treatment, Sirt5 KD BV2 cells exhibited increased generation of reactive oxygen species(ROS), accumulation of lipid droplets, and elevated levels of lipid peroxidation. By employing immunoprecipitation, introducing point mutation to critical succinylation sites, and conducting enzyme activity assays for succinate dehydrogenase(SDH) and trifunctional enzyme subunit alpha(ECHA), we demonstrated that succinylation plays a regulatory role in modulating the activities of these mitochondrial enzymes. Finally, down-regulation the succinylation levels achieved through administration of succinyl phosphonate(SP) led to amelioration of MG senescence in vitro and neuroinflammation in vivo. To our knowledge, our data provide preliminary evidence indicating that up-regulated succinylation modifications elicit a senescence phenotype in MG through alterations in energy metabolism. Moreover, these findings suggest that manipulation of succinylation levels may offer valuable insights into the treatment of aging-related neuroinflammation.

*Correspondence:
Jianmei Ma
ma_jianmei@hotmail.com

Full list of author information is available at the end of the article

Graphical abstracts

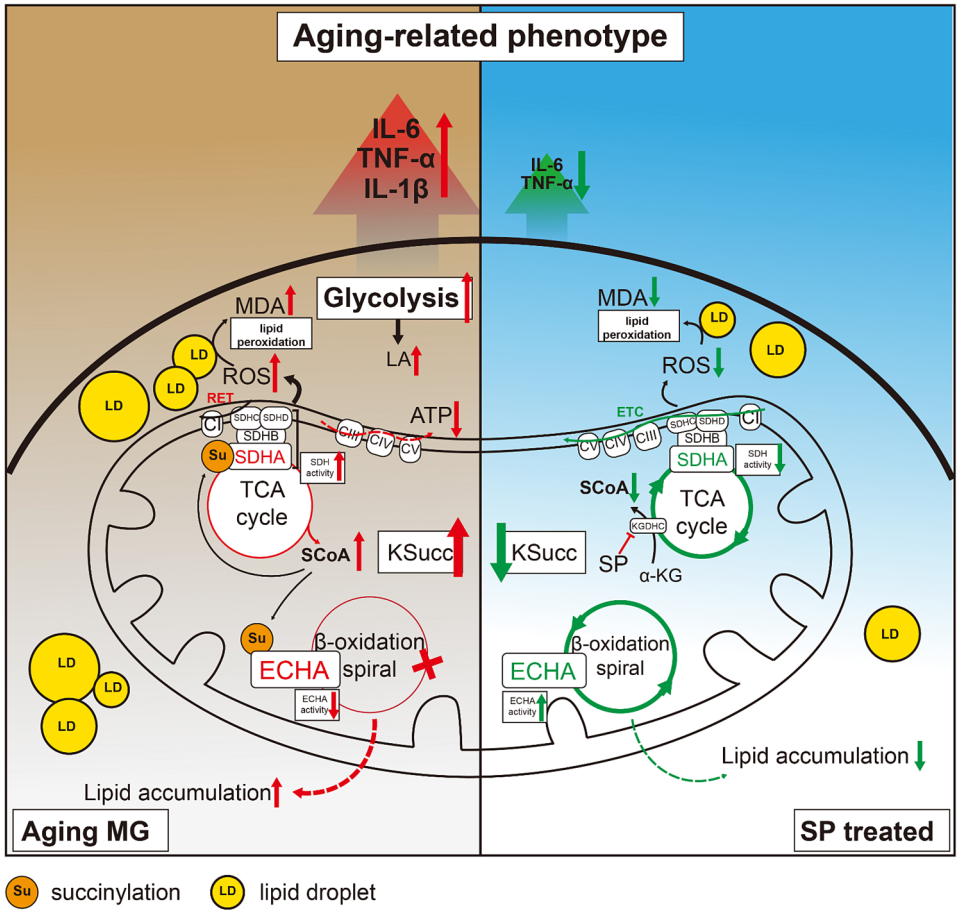

Keywords Succinylation, Aging, Microglia, Neuroinflammation, Metabolic reprogramming

Introduction

Epidemiological studies indicate a significantly higher incidence rate of neurodegenerative diseases among individuals over 65 years old, which has a profound impact on the health and daily life of elderly [1]. Aging related neuroinflammation, characterized by glial cell activation and increased production of pro-inflammatory cytokines in the central nervous system(CNS), is the frequent phenomenon closely associated with neurodegenerative diseases such as Alzheimer's disease(AD) and Parkinson's disease(PD) [2, 3]. Microglia(MG), the resident immune cells of CNS, play a crucial role in maintaining homeostasis of microenvironment, immune surveillance, synapse pruning and regulation of neuronal excitability [4, 5]. MG in the aging brain and neurodegenerative diseases can not only directly produce pro-inflammatory cytokines but also release various chemokines to promote peripheral circulating T lymphocytes and macrophages to enter the CNS through incomplete blood-brain barrier(BBB) [6, 7]. Thus, the activation of MG and continuous release of pro-inflammatory cytokines form a positive feedback loop, mediating long-term inflammatory responses associated with aging and diseases. Furthermore, by development of single-cell transcriptome studies, several distinct MG subpopulations such as lipid-droplet-accumulating MG(LDAM) and disease-associated MG(DAM) are identified. These subpopulations exhibit weakened phagocytic clearance ability and a decline in immune surveillance function. Conversely, they demonstrate a strong inflammatory response by releasing reactive oxygen species(ROS) and inflammatory factors, which promote aging brain neuron damage and neurodegenerative diseases [8–10].

MG can express key genes involved in multiple energy substrate metabolism pathways and flexibly regulate immune metabolism pathways to meet the diverse cellular energy needs of different microenvironments [11, 12]. Modulating MG's metabolic mode may alter its

immune function, potentially impacting the development and outcomes of diseases. It is well known that MG has two major functional phenotypes: the pro-inflammatory type, which is regarded as the neurotoxic phenotype, and the anti-inflammatory and neuroprotective type. Studies have demonstrated that changes in metabolic modes are related to the activation phenotype of MG. When exposed to pro-inflammatory media, MG can switch its energy metabolism mode from oxidative phosphorylation(OXPHOS) to glycolysis [12]. For instance, treatment of primary MG(PriMG) and microglial cell line BV2 with lipopolysaccharide(LPS) significantly increases cellular lactic acid(LA) level while decreasing adenosine triphosphate(ATP) production [13, 14]. Additionally, some studies have found that excessive division of MG mitochondria negatively regulates their respiratory function and OXPHOS level after LPS stimulation. The changes in energy metabolism mode related to the pro-inflammatory phenotype, similar to the Warburg effect observed in tumor cells, suggest an enhancement of glycolysis activity [15, 16]. In the anti-inflammatory activated status, research has revealed that it mainly enhances the OXPHOS level of cell mitochondria and fatty acid oxidation(FAO) as the predominant mode of energy metabolism [17, 18]. Within this series of regulation processes governing energy metabolism mode, mitochondria serve as the central hub connecting cellular energy metabolism with MG activated status.

Post-translational modifications(PTMs) play a crucial role in regulating protein functions, molecular interactions, and localization, all of which are associated with physiological and pathological processes [19]. Common types of modifications include acylation modifications such as acetylation, malonylation, succinylation, glutarylation, and palmitoylation [20–23]. The modifier groups of these acylation modifications all originate from intermediate products in cell energy metabolism, such as malonyl-CoA, glutaryl-CoA, and succinyl-CoA(SCoA), thereby closely linking these modifications to mitochondrial energy metabolism [24]. Among them, succinylation, a relatively recently discovered novel PTM, involves the modification of protein lysine groups by metabolically derived SCoA [25]. Succinylation of lysine induces more substantial alterations in a protein's chemical properties compared to methylation and acetylation, both of which are crucial post-translational modifications (PTMs) with essential cellular functions. At physiological pH (7.4), succinylation alters the charge of a lysine residue from +1 to −1, acetylation changes from +1 to 0, and monomethylation does not change it at all. Additionally, succinylation introduces a larger structural moiety (100.0186 Da mass shift) than acetylation (42 Da) or methylation (14 Da), leading to more pronounced alterations in protein structure and function [21]. Succinylation has been reported to be positively correlated with aging-related diseases such as premature ovarian failure and osteoporosis in menopausal women, suggesting that succinylation may be involved in the body's aging changes [26, 27]. The balance between succinylation and desuccinylation is maintained by the levels or the activities of modification writers and the erasers [28]. Succinylation is reported to occur spontaneously, which correlates with the SCoA concentration in the mitochondria. Sirtuin 5(Sirt5) is the only reported desuccinylase in all cell compartments but mostly localizes to the mitochondria. As a member of NAD+dependent lysine deacetylases, Sirt5 has been reported to play a crucial role in the aging process [29]. However, the effects of protein succinylation on MG activation and aging remain unknown.

In the present study, we used in vivo and in vitro aging models to detect levels of brain and cellular mitochondrial succinylation, as well as the cellular energy metabolism mode. We also revealed the effects of protein succinylation on MG energy metabolism and activation in CNS aging. Our findings provide a new direction for researching the mechanism of aging-related neuroinflammation and the intervening in CNS aging from the perspective of protein succinylation.

Materials and methods

Animals

Aged(17–20 months old) and young(2–4 months old) C57BL/6J male wildtype(WT) mice were obtained from Dalian Medical University. All mice were group housed at 22 ℃ on a 12-hour light /12-hour dark cycle with free access to food and water. All procedures were in accordance with the Dalian Medical University guidelines for the proper care and use of laboratory animals and were approved by the Laboratory Animal Care and Use Committee of Dalian Medical University.

LPS injections

2 to 4-month-old male WT mice were injected with LPS(from E. coli, Sigma), intraperitoneal injection(ip.) 1 mg LPS /kg body weight. Control mice were injected with body weight corresponding volumes of saline. 24 h after the LPS injection, mice were euthanized, and the brains were extracted and were processed for the following experiments. In the succinyl phosphonate(SP) administration experiment, mice were injected with LPS 24 h after the intracerebroventricular(icv.) injection of SP.

Intracerebroventricular (icv.) Injection

Mice were anesthetized with tribromoethanol and fixed to a stereotaxic apparatus(Stoelting Company, USA) and received right-unilateral injection of SP(1 mg/kg body weight) in a volume of 2 μL. The following coordinates

were used for central injection: 0.4 mm posterior, 1.0 mm right lateral, and 2.2 mm dorsoventral to bregma.

Perfusion and tissue preparation

Mice were anesthetized with tribromoethanol and perfused with 4% paraformaldehyde(PFA) solution(for cryogenic section) or cold PBS(for mitochondria isolation, protein and RNA extraction). For the cryogenic section, the brains were extracted, fixed in 4% PFA for 24 h, then cryoprotected in 20% sucrose solution for further procedures. For protein and RNA extraction, brains were perfused with cold PBS, tissues were collected according to different brain regions, then keep in the −80 ℃ freezer for further experiments.

Immunohistochemical(IHC) staining

The brains were removed and post-fixed overnight, then cryoprotected in 20% sucrose solution, embedded in optimal cutting temperature(OCT) compound(McCormick Scientific, St. Louis, MO, USA), and serial 16 μm sagittal sections were made with a cryostat(Leica CM 3050 S, Leica Microsystems AG, Wetzlar, Germany). IHC staining was performed as described previously [30]. The primary antibodies rabbit anti-Iba-1(Wako, Japan 1:500) and biotin-labeled secondary antibody(Vector Laboratories Inc., USA) were used. Images were captured using the Nikon digital camera system(DS-Fi1) in combination with microscopy(Nikon eclipse 80i).

Primary culture of MG

C57BL/6J mice at postnatal 48 h were used to prepare PriMG. Brain tissues were quickly removed, and the meninges were carefully stripped in ice-cold Dulbecco's Modified Eagle Medium(DMEM, Gibico). The tissues were then gently pipetted to generate single cells with DMEM followed by plating on poly-L-lysine-coated flasks. The culture medium was changed to fresh medium containing 10% FBS on day 3 and 10. After 14 days, PriMGs were collected from the mixed glial culture by shaking the flasks(250 rpm) for 4 h. The collected cells were seeded in the cultured plates and maintained at 37 ℃ with 5% CO_2.

BV2 cell culture and transfection

The mouse microglial cell line BV2 was cultured in DMEM containing 10% FBS and 1% penicillin/streptomycin(Hyclone). Cells were maintained in the incubator at 37℃ with 5% CO_2. Cells were plated at a density of 1×10^5/well in a six-well plate or 4×10^5 in 60-mm dishes 18 h before transfection. Transfection was performed using Lipofectamine 3000 transfection reagent(Thermo Fisher) and follow the manufacturer's instruction.

Generation of Sirt5 stable knockdown(KD) cell lines

BV2 cell line was maintained in DMEM supplemented with 10% FBS and 1% penicillin/streptomycin(Hyclone) at 37 °C with 5% CO_2. To establish the stable Sirt5 KD BV2 cell line, two sgRNAs targeting the coding region of mouse Sirt5 gene and non-coding(NC) sgRNA as NC control were synthesized and employed to construct lentivirus recombinant vector(Genechem Co Ltd, China). BV2 cells were divided into control, NC transfection and Sirt5 KD transfection groups. Prior to transfection, cells were planted in 24-well plates and allowed to develop to 90% confluence. Polybrene(5 μg/mL) was added to improve transfection efficiency. To obtain stable infected cells and avoid the stimulation of traditional purinomycin purification of BV2 cells, fluorescence-activated cell sorting(FACS) was carried out to sort the enhanced green fluorescent protein(EGFP) positive cells. Cells were collected for subsequent experiments.

Isolation of mitochondria

Mitochondria from mouse hippocampus, primary microglia and BV2 cells were isolated using Minute™ mitochondria isolation kit(MP-007, Invent Biotechnologies) according to the manufacturer's instructions. The isolated mitochondria samples were then kept in Minute™ denatured or non-denatured protein solution and then stored at -80 ℃ for western blot analyses.

Immunoprecipitation(IP) and Western blot(WB)

Cell and tissue samples were lysed in RIPA lysis buffer(KeyGEN, China) containing protease inhibitors(PMSF; Biosharp, China) and phosphatase inhibitor cocktail(Med Chem Express, China) on ice for 30 min and centrifuged for 15 min at 16,000 ×g. The concentrations of proteins were determined with BCA Protein Assay Kit(KeyGEN, China). For the IP experiment, the samples(1 mg) were incubated with anti-SDHA(4 μg) and anti-ECHA(4 μg) or anti-IgG antibody and protein A/G-agarose overnight at 4 °C. After washing, the bound proteins were eluted from the beads by boiling in sample buffer and subjected to WB analysis.

For Wb analysis, samples were separated by 5–20% polyacrylamide gels(KeyGEN, China), then transferred to a nitrocellulose membrane(NC; Pall Corporation, Mexico). The blots were blocked in 5% BSA(Gentihold, China) for one hour at room temperature(RT), and incubated with primary antibodies overnight at 4 °C. Then incubated with fluorescence labeling secondary antibody(1:15000; LI-COR, USA) for one hour at RT. The bands analyzed and quantified using an Odyssey CLx Imager and Image Studio software(LI-COR, USA). Ponceau S staining of the protein after blotting was used for normalization(listed in the supplementary Fig. 1). The range of the WB measurement of succinylation is from

10 KD to 100 KD, and the range of each gel has been marked on the figure in supplementary Fig. 1. The primary antibodies used in assays were listed in the supplementary table.

Quantitative real-time PCR(qPCR)

Total cellular RNA was extracted using Trizol reagent(Thermo Fisher Scientific, USA) according to the manufacturer's protocol. The concentration of RNA was quantified by ultraviolet spectrophotometry at 260/280 nm(Nanodrop 2000, Thermo scientific, USA). The Script First-Strand c-DNA Synthesis SuperMix Kit(Takara, Japan) was used to transcribe cDNA. PCR was performed on a Mx3000P(Agilent, USA) quantitative real-time detection system with corresponding primers and SYBR green PCR master mix(Takara, Japan). The target gene expression was calculated as $2-\Delta\Delta Ct$ method. Forty cycles of PCR amplification were performed as follows: denature at 95 °C for 30 s, anneal at 55 °C for 30 s, and extend for 30 s at 72 °C. All primers were synthesized by Invitrogen, the primers were listed in the supplementary table.

Measurement of ATP and LA level

The whole lysate and mitochondrial protein of cultured cell line were collected. All samples were immediately stored at −80 °C until assay. The assay was performed according to ELISA Kit protocols of ATP, and LA(ENOVA, China). Cytation 5(BioTek, USA) was used to measure absorbance at 450 nm.

Seahorse extracellular flux assays

Seahorse XF Glycolytic rate assay kit, Seahorse XF Cell Mito Stress Test Kit, Seahorse XF real-time ATP production rate kit and the Seahorse Extracellular Flux(XF96) Analyzer was used to analyze cell bioenergetics. BV2 cells(3×10^5 cells/well) were seeded on Seahorse cell culture microplates and incubated in DMEM. After LPS treatments, ECAR and OCR were measured according to the manufacturer's protocol. For the glycolytic rate assay, Rotenone plus Antimycin A(Rot/AA, 5 μM) and 2-deoxy-D-glucose(2-DG; 500 mM) were prepared in glycolytic flux assay media and similarly loaded into the appropriate ports. For the mito stress test, oligomycin(15 μM), FCCP(2 μM), and Rot/AA(5 μM) were loaded into the appropriate ports for sequential delivery. For the real-time ATP production test, oligomycin(15 μM) and Rot/AA(5 μM) were loaded into the appropriate ports. Following calibration, OCR and ECAR were measured every 3 min for 84 min, and the appropriate compounds were injected sequentially. ECAR and OCR were automatically calculated using the Wave software(Agilent Technologies, USA), and three replicates were assessed for each separate sample. Data normalization was performed by Cytation 5(BioTek, USA).

MitoSox assay

The stock solution(5 mM) of MitoSox was prepared by dissolving the contents of the vial in 13 μL DMSO. To make the working solution(500 nM), add 5 μL of 5 mM stock solution to 50 mL of HBSS with Ca^{2+} and Mg^{2+}. Cells were incubated with the working solution for 30 min at 37 ℃ and 5% CO_2. Cells were analyzed by flowcytometry(FC) or fluorescence microscopy, and three replicates(three different passages of the cell) were assessed for each separate sample. The MitoSox Ex/Em at 396/610 nm and was detected at 488/594 nm.

Nile red assay

Stock solution of Nile red(10 μg/ mL) in acetone were prepared and stored protected from light. The dye was then added directly to the preparation to affect a 1:100 dilution and incubated with cell for 30 min protected from light. Then analysis immediately by FC(561/579 nm) or fluorescence microscopy (594 nm), and three replicates(three different passages of the cell) were assessed for each separate sample.

Mito red tracker assay

The stock solution of Mito Red Tracker was prepared by dissolving the contents of the vial in 20 μL DMSO. Collected approximately 1×10^6 cells in suspension to each flow cytometry tube. Cells were resuspended in 1mL PBS and Mito Red tracker dye was added 1 μL/tube. Cells were incubated at 37 ℃ and 5% CO_2 for 30 min protected from light. Cells were then analyzed by FC at 561/640 nm with three replicates(three different passages of the cell) were assessed for each separate sample.

Activity assay of succinate dehydrogenase complex(SDH)

The cell mitochondrial protein was subjected to SDH enzyme activity test. According to the manufacturer protocol, the working solution was put into the incubator at 37℃ to preheating for 10 min. Add 180 μL working solution and 10 μL sample solution to the well and mix fully. In control group, add 180 μL working solution and 10 μL water to the well. Measure the absorbance value(595 nm) at the beginning and 1 min later, respectively. Calculate SDH enzymatic activity according to the kit instruction(Solarbio Technology Co., China).

Activity assay of trifunctional enzyme subunit alpha(ECHA)

The ECHA activity was detected as previously described [31]. The reaction mixture contained 100 mM Tris-HCL(pH 9.0), 100 mM KCL, 100 μg/ mL BSA, 120 μM NAD+, and 30 μM DL-3-Hydroxybutyryl coenzyme A as the substrate. The activity was measured by monitoring

the formation of NADH at 340 nm for 10 min by Cytation 5(BioTek, USA).

Untargeted metabolomics

Culture medium was removed from cultured BV2 cells. Then the cells were washed with PBS under 37 ℃ and the PBS was removed. 800 μL of cold methanol(Fisher, USA)/ acetonitrile(Merck, USA) (1:1, v/v) to remove the protein and extract the metabolites. The mixture was collected into a new centrifuge tube and centrifuged at 14,000 ×g for 20 min to collect the supernatant. The supernatant was dried in a vacuum centrifuge. For LC-MS analysis, the samples were redissolved in 100 μL acetonitrile/ water(1:1, v/v) solvent and centrifuged at 14,000 ×g at 4 ℃ for 15 min, then the supernatant was injected. The further LC-MS/MS analysis was performed using an UHPLC(1290 Infinity LC, Agilent Technologies) coupled to a quadrupole time-od-flight(AB Sciex TripleTOF 6600) in Shanghai Applied Protein Technology Co., Ltd. The raw MS data were converted to MzXML files using ProteoWizard MSConvert before importing into freely available XCMS software. For peak picking, the following parameters were used: centWave m/z=10 ppm, peakwidth=c(10, 60), prefilter=c(10, 100). For peak grouping, bw=5, mzwid=0.025, minfrac=0.5 were used. CAMERA(Collection of Algorithms of MEtabolite pRofile Annotation) was sued for annotation of isotopes and adducts. In the extracted ion features, only the variables having more than 50% of the nonzero measurement values in at least one group were kept. Compound identification of metabolites was performed by comparing of accuracy m/z value (<10 ppm), and MS/MS spectra with an in-house database established with available authentic standards.

Statistical analysis

All data results were expressed as the mean±standard error of the mean(SEM). All data were analyzed using GraphPad Prism 9.0 software. Differences among the groups were evaluated using one-way analysis of variance, followed by Tukey's honest significance test. Paired student's t test was used to compare the differences between two groups. The P values<0.05 were considered to be significant.

For the untargeted metabolomic data analysis, after sum-normalization, the processed data was analyzed by R package (ropls), where it was subjected to multivariate data analysis, including orthogonal partial least-squares discriminant analysis(OPLS-DA). The 7-fold cross-validation and response permutation testing were used to evaluate the robustness of the model. The variable importance in the projection(VIP) value of each variable in the OPLS-DA model was calculated to indicate its contribution to the classification. Student's T test was applied to determine the significance of differences between two groups of independent samples. VIP>1 and p value<0.05 were used to screen significantly changed metabolites. Pearson's correlation analysis was performed to determine the correlation between two variables.

Results

Succinylation level was increased in aging or activated MGs combined by metabolic reprogramming

To investigate the changes of succinylation modification during aging, we collected hippocampus tissues from six young(4 months) and nine aged(from 17 months to 20 months) male mice brains for the further experiments(Fig. 1A). First, the level of succinylation in the mitochondria proteins of the hippocampus tissues was compared by WB, as succinylation is particularly abundant in mitochondrial metabolic pathways [28]. The results showed that the succinylation level was significantly increased in aged mice(Fig. 1Ba). Next, total RNA was exacted from hippocampus and qPCR analysis was performed to detect the expression of pro-inflammatory cytokines. The result showed that tumor necrosis factor alpha(*Tnf-α*) was significantly increased in the aged mice compared to young mice(Fig. 1Bb). While the level of interleukin-1beta(*Il-1β*) expression showed an upward trend and the *Il-6* expression showed no difference between the young and old mice(Fig. S2B). Simultaneously, "rod-shaped"(with enlarged cell body and polarized processes) and "dystrophic"(enlarged cell body and retracted processes) MGs with were detected in cortex and hippocampus of aged mice by Iba-1 IHC staining(Fig. 1C and S2A). These results indicate that as increasing neuroinflammation in the aging brain, the level of succinylation in mitochondria is elevated.

Since dystrophic MGs and elevated mitochondrial succinylation were found in aging brain, we wondered whether mitochondrial succinylation occurs in aging MGs. Therefore, we used 21-day cultured PriMGs(Fig. 1Da) (which has been previously described as an in vitro model of aged PriMG) [32], and BV2 cells treated with Etoposide(VP16) to mimic nature aging and DNA damage-induced aging of MGs [33]. After the long-term culture, the 21-day PriMGs exhibited more significant senescence than those cells cultured for 3-day, as evidenced by increased expression of cyclin dependent kinase inhibitor 2 A(*Cdkn2a*, *p16*) along with DNA damage(Fig. 1Db). Furthermore, a cluster of genes correlated with DAM, which were also discovered recently in the aging MGs, such as tyrosine-protein kinase receptor UFO(*Axl*) and triggering receptor expressed on myeloid cells 2(*Trem2*), were significantly increased in 21-day PriMGs, verifying their aging status(Fig. 1Db) [34]. Interestingly, the succinylation level in the mitochondria of 21-day PriMGs was also significantly increased

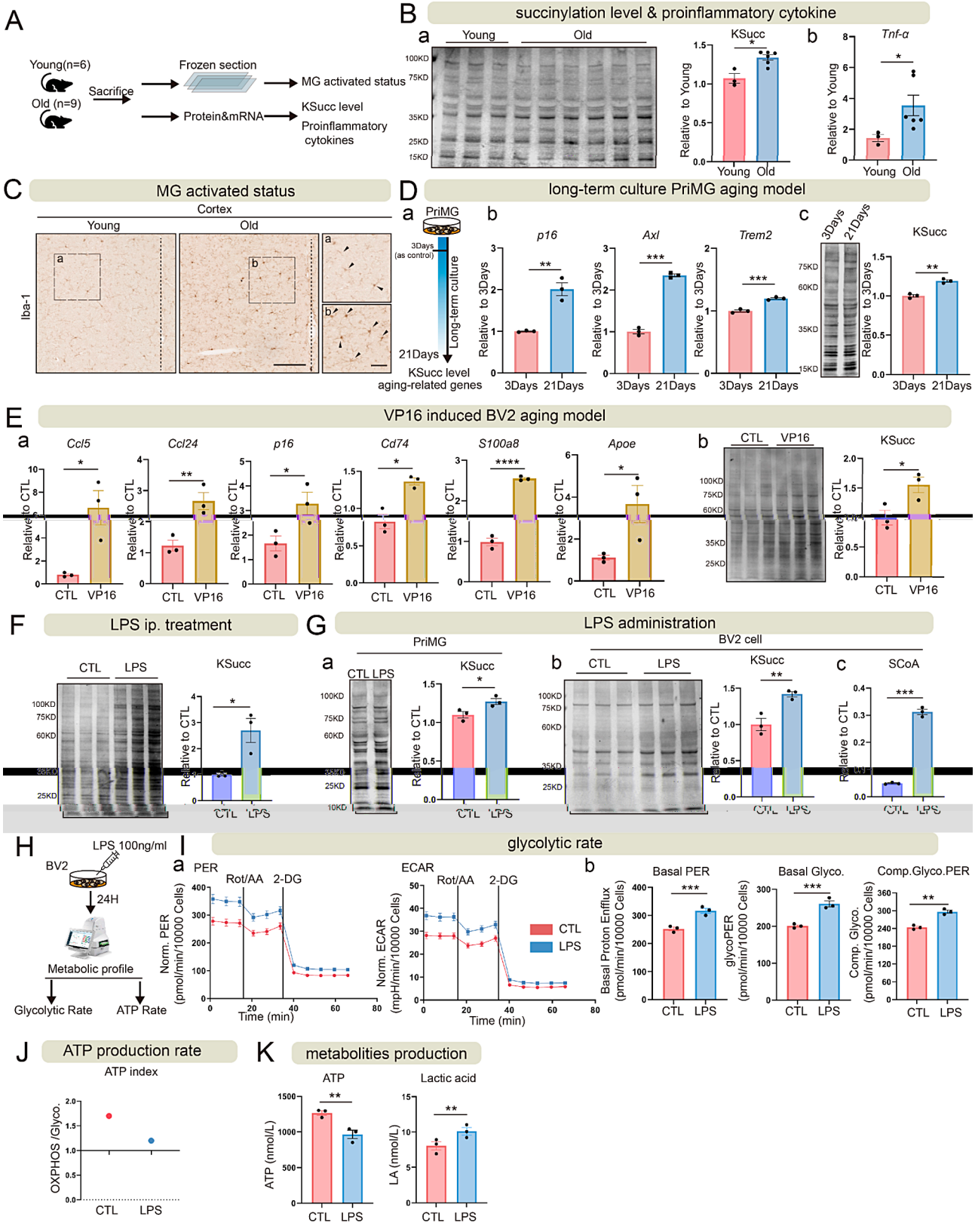

Fig. 1 (See legend on next page.)

(See figure on previous page.)

Fig. 1 Succinylation level was increased in aging or activated MGs acompanied by metabolic reprogramming. **(A)** Schematic experimental workflow for the identification of succinylation level, MG activated status, neuroinflammation level in the aging mice. **(B)** Succinylation level and neuroinflammation level of the aging mice.(young: $n=3$ and aging $n=6$); **(a)** Succinylation level between the young and aging mice confirmed by WB; **(b)** Proinflammatory cytokine *Tnf-a* transcription level evaluated by qPCR. **C.** MG activation states in the cortex (×20) and inset (×40) confirmed by IHC. Bar = 500 μm(×20) and 100 μm(×40). **D.** Succinylation level and aging-related genes in the long-term culture PriMG aging model; **(a)** Schematic of the long-term culture model; **(b)** Aging-related genes detected by qPCR; **(c)** Succinylation level between 3-day and 21-day cultured PriMG confirmed by WB. **E.** Succinylation level and aging-related genes in the VP16 induced MG aging model; **(a)** Aging-related genes detected by qPCR; **(b)** Succinylation level between CTL and VP16 treated groups confirmed by WB. **F.** Succinylation level in the mitochondrial lysate of hippocampus between CTL and LPS treated mice in the ip. treatment model. **G.** Succinylation level and SCoA concentration in the LPS treated PriMG and BV2 cells; **(a)** Succinylation level between CTL and LPS treated PriMGs confirmed by WB; **(b)** Succinylation level between CTL and LPS treated BV2 cells confirmed by WB; **(c)** The concentration of SCoA in cellular total lysate detected by colorimetric method. **H.** Schematic of the metabolic profile detected by Seahorse XF96 analyzer. **I.** The glycolytic rate changes following LPS treatment detected by the glycolytic rate assays. **J.** The ATP production rate changes following LPS treatment detected by the real-time ATP production rate assays. **K.** The levels of ATP and LA in cellular total lysate detected by ELISA. $n=3$/group, * $P<0.05$, ** $P<0.01$, *** $P<0.005$, **** $P<0.001$

compared to those 3-day cultured cells(Fig. 1Dc). As the DNA damage induced aging model, VP16 was administered to the BV2 cells for 7 days. After that, the expression of chemokine(C-C motif) ligand 5(*Ccl5*) and *Ccl24*, which are genes associated with the senescence-associated secretory phenotype(SASP), was demonstrated significantly increased compared to control cells(Fig. 1Ea) [35]. Additionally, *p16* was also increased after the treatment(Fig. 1Ea). Furthermore, the expression of specific aging-related genes that have been recently reported, such as HLA-DR antigens-associated invariant chain(*Cd74*), S100 calcium-binding protein A8(*S100a8*) and apolipoprotein E(*Apoe*), were upregulated in the VP16-treated cells(Fig. 1Ea). Additionally, we observed an increase in the number of senescence-associated β-galactosidase(SA-β-Gal)-positive BV2 cells following the VP16 treatment(Fig. S2B). Similar to PriMGs, the succinylation level in the mitochondria of BV2 cells also significantly elevated after VP16 treatment(Fig. 1Eb). These findings demonstrate that the succinylation level is elevated in the aging MGs.

Chronic inflammation, a defining characteristic of aging brain, is closely linked with aged MGs [36]. To know the succinylation state in the brain during inflammation, we established in vivo and in vitro neuroinflammation models by LPS administration. After 24 h of LPS ip. treatment(1 mg/kg), the level of mitochondrial proteins succinylation in hippocampus was nearly three times higher than that in control mice(Fig. 1F). Consistent with our in vivo experiments, we also found a significant increase in succinylation levels within mitochondria after treating both PriMGs and BV2 cells with LPS for 24 h(Fig. 1Ga and Gb). Meanwhile, SCoA levels, which serve as a source of protein succinylation [37], were more than three times higher in LPS-treated BV2 cells compared to control cells(Fig. 1Gc). These results indicate that the succinylation level is increased in the inflamed brain and the activated MGs.

Given that the status of immune cells is reflected in their cellular metabolism, and succinylation modification has been reported to mainly occur in the mitochondria which was associated with energy metabolism [28, 38], the real-time cell metabolic analysis was performed by using Seahorse XFe96 analyzer, including glycolytic rate and ATP production rate in BV2 cells with or without LPS treatment(Fig. 1H). The results showed that the normalized ECAR and PER were significantly elevated in LPS treated cells than that in control cells(Fig. 1Ia), and the basal proton efflux rate(basal PER), basal glycolysis(glyco. PER) and the compensate glycolysis(Comp. Glyco.) also increased significantly(Fig. 1Ib). These results indicate an aggressive shift toward glycolytic metabolism during MG activation. Furthermore, by real-time ATP rate assay, ATP index(the ratio of oxidative phosphorylation ATP(OXPHOS) and glycoATP(Glyco.)) was calculated in both control and LPS-treated BV2 cells. The results showed that the ATP index, as shown in Fig. 1J, was above 1.5 and nearly 2.0 in control cells, suggesting that OXPHOS is the main cellular energy production manner in untreated cells. However, the ATP index was significantly reduced in LPS-treated cells, suggesting the energy metabolic mode changed from OXPHOS to glycolysis when BV2 cells were in activated status(Fig. 1J). Furthermore, we measured the intracellular concentration of ATP and LA. We found that the ATP concentration of LPS-treated cells was significantly reduced, accompanied by an increased LA concentration compared to control cells(Fig. 1K). These results indicate the metabolic reprogramming occurs during MG activation.

Upregulated succinylation induced by Sirt5 KD results in MG senescence phenotype accompanied by alterations in energy metabolism

To gain deeper insight into the relationship between succinylation modification and MG senescence, lentivirus mediated transfection of a CRISP-Cas9 KD system was employed to introduce two different Sirt5 sgRNAs(LV-68 and 70), as well as a noncoding sgRNA(LV-NC) (Fig. 2A). This approach aimed to generate a stable Sirt5 KD BV2 cell line for manipulating the succinylation state because Sirt5 is considered as the unique enzyme in mitochondria that regulates succinylation [29]. In the experimental procedure depicted in Fig. 2A, transfected cells were assessed by FC, and EGFP-positive cells were sorted

and collected via FACS for subsequent experiments. To verify Sirt5 KD efficiency, WB analysis was performed, and the result showed successful downregulation of Sirt5 expression was achieved following LV-68 and LV-70 transfection(Fig. 2B). We selected LV-70 Sirt5 KD BV2 cells for the subsequent experiments. Consistently, both the total lysate and the mitochondria lysate from these cells exhibited the significantly elevated levels of succinylation(Fig. 2C). To investigate whether the upregulation of succinylation induced by Sirt5 KD contributes to MG senesces, we subsequently examined specific genes associated with MG aging, including *Axl*, *Ccl24*, ferritin heavy chain 1(*Fth1*), and *Ccl5*(Fig. 2Da). The results exhibited that these aging-related genes were upregulated in Sirt5 KD BV2 cells, except for *ccl5*. Additionally, the expression of DAM-related genes C-type lectin domain family 7 member A(*Clec7a*) and *Trem2* was also elevated in the Sirt5 KD cells, resembling their expression patterns observed in aging MGs(Fig. 2Db). Besides changes in genes expression related to aging, both the proliferation rate and the cellular ATP level of the Sirt5 KD cells decreased compared to control cells(Fig. 2Ea, b). Overall, these findings suggest that hypersuccinylation induced by Sirt5 KD closely resembles the characteristics of aging MGs.

Furthermore, we performed real-time cell metabolic analysis including mitochondrial stress, glycolytic rate, and ATP production rate, to determine the metabolic profile of Sirt5 KD BV2 cells. First, for the mitochondrial stress test, the cell OCR was measured using Seahorse XFe96 analyzer. The results showed that under basal conditions(Basal resp.), the normalized OCR(Norm. OCR) of Sirt5 KD cells was slightly higher than that of control cells. However, after treatment with inhibitors including oligomycin(Oligo), FCCP, rotenone(Rot) and antimycin A(AA), there was no significant difference in OCR level between Sirt5 KD and control cells(Fig. 2Fa). Furthermore, we found that Sirt5 KD cells exhibited a significantly reduced mitochondrial spare capacity(Spare Capa.) and a significantly increased proton leak level compared to the control cells(Fig. 2Fb), suggesting that elevated succinylation induced by Sirt5 KD decreased adaptability of mitochondria. Next, for the glycolysis rate assay, we observed significantly higher levels of ECAR and PER in Sirt5 KD cells compared to control cells(Fig. 2Ga). Simultaneously, the Basal PER Basal Glyco. and Comp. Glyco PER were also significantly higher in Sirt5 KD cells compared to control cells(Fig. 2Gb), suggesting an energy production shift towards glycolysis caused by elevated succinylation modification induced by Sirt5 KD. Thirdly, for ATP production rate assay, we measured the ratio of ATP production between OXPHOS and Glyco. The results indicated a slightly lower rate in Sirt5 KD cells compared to the control cells(Fig. 2H). However, glycoATP production was significantly increased in Sirt5 KD cells(Fig. 2H). These data suggest that elevated succinylation modification induced by Sir5 KD leads to metabolic reprogramming with decreased OXPHOS and increased glycolysis level, as well as a weakening of mitochondrial adaptability.

Upregulated succinylation modification enhances inflammatory susceptibility of MGs accompanied by excessive ROS production and disturbed lipid metabolism

In the aforementioned results, Sirt5 KD BV2 cells exhibited significantly elevated succinylation levels and displayed characteristics resembling those of aging MGs. Given this status, it is important to investigate how MGs react when they are subjected to an inflammatory attack, which is similar to elderly individuals suffering from inflammatory stimulation [39]. Therefore, we designed the experiment depicted in Fig. 3A, where we treated the control and Sirt5 KD BV2 cells with LPS respectively and compared them in terms of succinylation levels, metabolic function, ROS production, lipid accumulation, and activated status. The succinylation levels analyzed through WB of both total lysate and mitochondrial lysate after LPS treatment showed a significant increase and was more pronounced in Sirt5 KD cells(Fig. 3B). In terms of metabolic functions assessed through glycolytic rate and ATP production rate test, it is interesting to note that ECAR and PER did not exhibit a further increase in Sirt5 KD cells after LPS treatment but were increased in the control cells after LPS treatment(Fig. 3C). However, the proportion of ATP produced by glycolysis was increased after LPS treatment in Sirt5 KD cells, accompanied by a significant decrease in ATP index(Fig. 3D). These results demonstrate that under inflammatory conditions, there is a significant shift toward glycolysis as the primary energy metabolic mode in Sirt5 KD BV2 cells.

Aging MGs are one of the primary sources of increased ROS levels in the aging brain, and excessive production of microglial ROS may contribute to aging-related CNS dysfunctions [40]. Therefore, the level of mitochondrion ROS(mtROS) was detected using MitoSOX staining, and the mean fluorescence intensity(MFI) was measured by FC. We found that the MitoSOX MFI level was significantly elevated in Sirt5 KD cells(Fig. 3E), supporting previous results indicating an increase in proton leak in these cells(Fig. 2F). Additionally, following LPS treatment, MitoSOX MFI was further increased in the Sirt5 KD cells compared to control cells(Fig. 3E).

The MGs of aging mice and human brains were found to exhibit a striking accumulation of lipid droplets, known as LDAM. These MGs demonstrate prominent characteristics such as elevated levels of ROS production and secretion of pro-inflammatory cytokines, which closely resemble the Sirt5 KD BV2 cells with upregulated

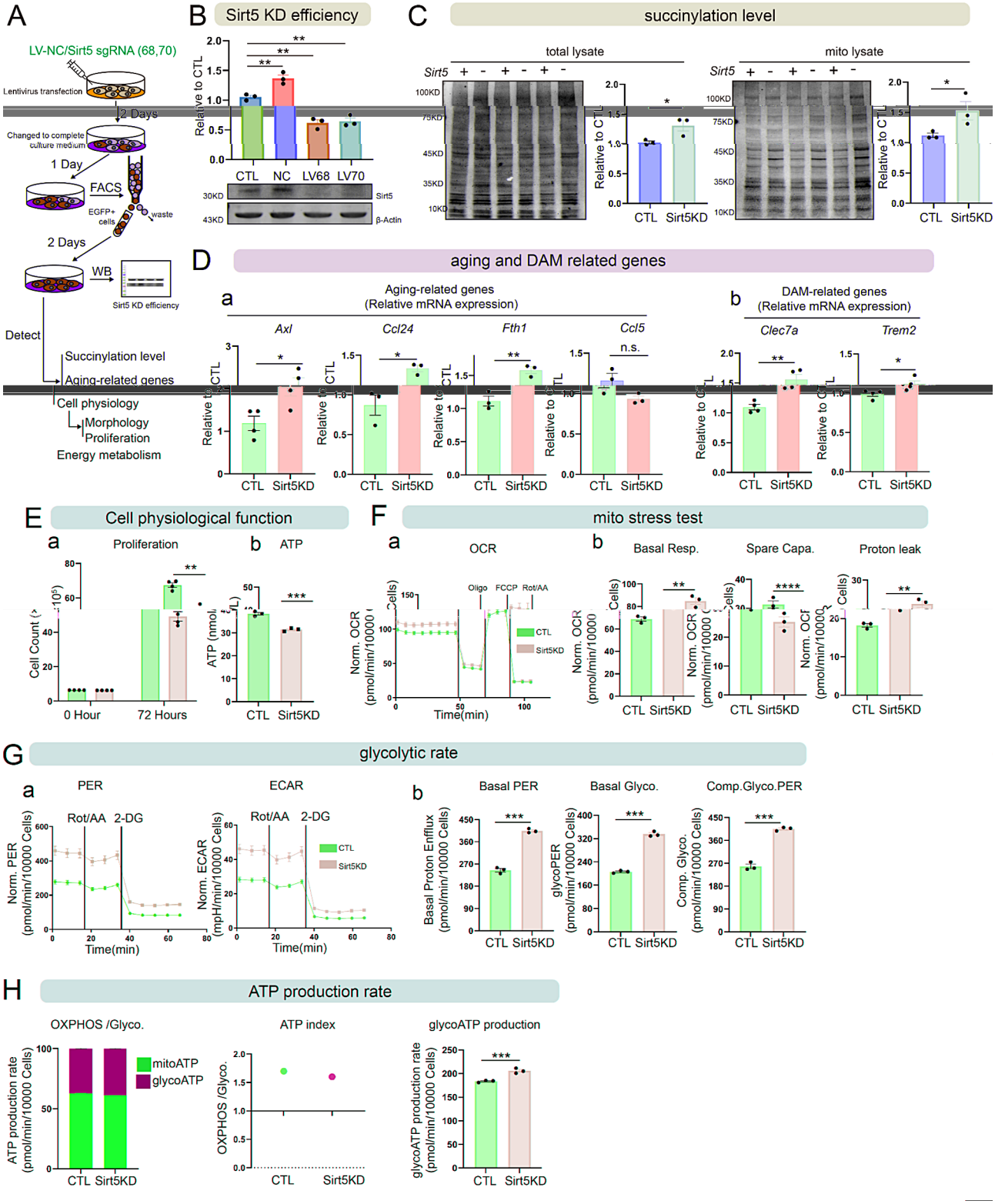

Fig. 2 (See legend on next page.)

(See figure on previous page.)

Fig. 2 Sirt5 KD-induced succinylation upregulation leads to microglial senescence and metabolic changes. **(A)** Schematic experimental workflow of the construction of stable Sirt5 KD BV2 cell line and further experiments. **(B)** Sirt5 KD efficiency after the LV transfection confirmed by WB. **(C)** Succinylation level between CTL and Sirt5 KD BV2 cells in **(a)** total lysate and **(b)** mito lysate detected by WB. **D.** Aging and DAM-related genes transcription levels between CTL and Sirt5 KD detected by qPCR. **E.** Cell physiological changes after Sirt5 KD; **(a)** The proliferation changes after the Sirt5 KD cells compared by absolute cell count by BioTek Cytation5 analyzer, **(b)** The levels of ATP in cellular total lysate detected by ELISA. **F.** The mito stress tests following Sirt5 KD; **(a)** Normalized OCR; **(b)** basal respiration rate(Basal Resp.), Spare capacity(Spare Capa.) and Proton leak were calculated. **G.** The glycolytic rate changes following LPS treatment detected by the glycolytic rate test. **(a)** normalized PER and ECAR; **(b)** Basal PER, Basal Glycolysis rate and compensate glycolysis PER were calculated. **H.** The ATP production rate changes following LPS treatment detected by the real-time ATP production rate assays. $n = 3$/group, * $P < 0.05$, ** $P < 0.01$, *** $P < 0.005$, **** $P < 0.001$

succinylation [8, 41]. Therefore, we detected the lipid droplets using Nile Red(NR) staining and the MFI was measured by FC in both control and Sirt5 KD BV2 cells. Surprisingly, the NR MFI of Sirt5 KD cells were significantly higher compared to control cells(Fig. 3F). Furthermore, following LPS treatment, the NR MFI level was significantly increased in both control cells and Sirt5 KD cells, with a higher level exhibited in Sirt5 KD cells(Fig. 3F). These results demonstrate that upregulated levels of succinylation increase the concentration of ROS and the accumulation of lipid droplets, which can be further exacerbated under inflammatory conditions.

Lipid peroxidation leads to the generation of toxic lipid products, such as malondialdehyde(MDA) and 4-hydroxy-2-nonenal(4-HNE), which contribute to neurodegeneration and aging [42–44]. Therefore, we measured the concentration of MDA in BV2 cells with or without LPS treatment using a colorimetric method. Surprisingly, the MDA level exhibited no change in the Sirt5 KD cells without LPS-treatment. After LPS treatment, control cells showed a slight increase, while a significant increase was observed in the LPS-treated Sirt5 KD BV2 cells(Fig. 3G). These results suggest that under inflammatory conditions, Sirt5 KD BV2 cells experience severe oxidative stress manifested by increased levels of lipid peroxidation.

Furthermore, the expression profile of different activated markers was determined by qPCR in control and Sirt5 KD cells with or without LPS treatment to assess the activated status of MGs. No significant difference was found between Sirt5 KD BV2 cells and control cells without any stimulation(Fig. 3H). However, a significant increase in expression of pro-inflammatory markers, including *Il1-1β*, *Il-6* and *Tnf-α*, were observed in LPS-treated Sirt5 KD BV2 cells(Fig. 3H). The expressions of anti-inflammatory markers such as transforming growth factor beta(*Tgf-β*), arginase 1(*Arg-1*) and *Il-4* had no significant differences between control and Sirt5 KD BV2 cells with or without LPS treatment (Fig. S2D). These findings suggest that elevated succinylation leads to improvement of inflammatory susceptibility of MGs.

To determine the effects of hypersuccinylation state on MG metabolism, we conducted untargeted metabolomics in the control and Sirt5 KD BV2 cells(Fig. 3I). First, OPLS-DA models were established to investigate the distribution of metabolites. The generated OPLS-DA model showed a distinct discrimination between the metabolic profiles of control and Sirt5 KD BV2 cells (Fig. 3J), thereby indicating significant differences in metabolites. Through a detailed comparison, we observed an enrichment of long-chain saturated and unsaturated lipids(Pg 30:0, Pg 32:1, Pg 40:7, Pe 36:4, Pe 38:5), as well as oxygenated lipid(pe(18:1/9-hode)), in the Sirt5 KD cells; conversely, there was a reduction in palmitic acid and oleic acid(Fig. 3K). It is also worth noting that a series of metabolites related to cholesterol metabolism, such as 7α-hydroxy-3-oxo-4-cholestenoic acid(7-HOCA) and isodeoxycholic acid were decreased significantly after Sirt5 KD(Fig. 3K). This may indicate that Sirt5 and succinylation play an important regulatory role in the regulation of microglial cholesterol metabolism-related pathways. Furthermore, we categorized the differential metabolites based on their superclass and quantified the number of up-regulated and down-regulated metabolites. Specifically, there were 46 down-regulated and 35 up-regulated differential metabolites. Among them, the most pronounced alterations were observed in lipids and lipid molecules, with 29 upregulated and 15 downregulated(Fig. 3L). Apart from lipids, a significant downregulation was predominantly observed in organic acids and their derivatives, organic heterocyclic compounds, as well as nucleosides, nucleotides, and analogues(Fig. 3L). These findings suggest that lipids are primarily impacted, resulting in an accumulation of long-chain lipids in Sirt5 KD BV2 cells.

To clarify the metabolic pathways predominantly affected in Sirt5 KD cells, we enriched the specific metabolites from various metabolic pathways. Our analysis revealed that down-regulated metabolites were particularly enriched in the 'Biosynthesis of unsaturated fatty acids' and 'Fatty acid biosynthesis' pathways(Fig. 3M). Conversely, up-regulated metabolites showed significant enrichment in the 'Glycolysis/Gluconeogenesis' and 'Glucagon signaling pathway'(Fig. 3M). These findings corroborate previous results indicating perturbed lipid metabolism and heightened glycolytic activity in Sirt5 KD BV2 cells.

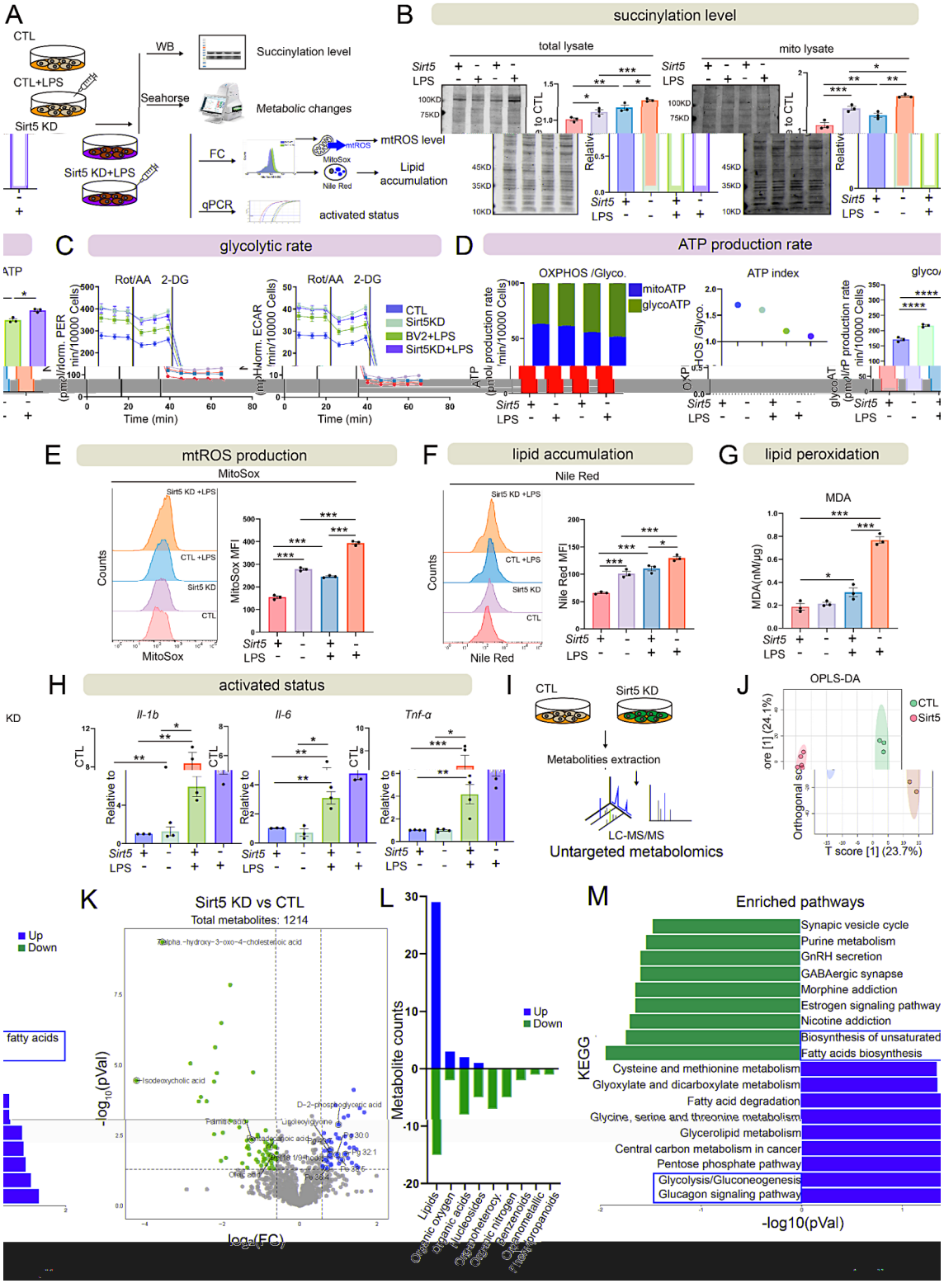

Fig. 3 (See legend on next page.)

(See figure on previous page.)

Fig. 3 Increased succinylation leads to enhanced MGs' inflammatory susceptibility, ROS over-production, and lipid metabolism disruption. **(A)** Schematic experimental workflow of Sirt5 KD BV2 cells with LPS treatment and further experiments. **(B)** Succinylation level between CTL and Sirt5 KD BV2 cells with LPS treatment in **(a)** total lysate and **(b)** mito lysate detected by WB. **C.** The glycolytic rate changes of CTL and Sirt5 KD cells following LPS treatment detected by the glycolytic rate test. **D.** The ATP production rate changes of CTL and Sirt5 KD cells following LPS treatment detected by the real-time ATP production rate assays. **E.** mtROS generation of CTL and Sirt5 KD cells treated with LPS detected by FC. **F.** Lipid accumulation of CTL and Sirt5 KD cells treated with LPS detected by FC. **G.** MDA concentration of CTL and Sirt5 KD cells treated with LPS detected by colorimetric method. **H.** Pro-inflammatory cytokines transcription levels of *Il-1β*, *Il-6* and *Tnf-α* in the CTL and Sirt5 KD cells treated with LPS detected by qPCR. **I.** Schematic workflow of non-targeted metabolomics. **J.** OPLS-DA analysis of non-targeted metabolomic datasets between CTL and Sirt5 KD cells. ($n=6$/group) **K.** Volcano plot showing different metabolites in CTL and Sirt5 KD cells ($n=6$/group). **L.** The counts of up and downregulated of different metabolites classified by superfamily. **M.** KEGG enrichment of different metabolites in CTL and Sirt5 KD BV2 cells. Upregulated metabolites are in red, and downregulated genes are in blue. $n=3$/group, * $P<0.05$, ** $P<0.01$, *** $P<0.005$, **** $P<0.001$

The activity of SDH and ECHA is regulated by succinylation modification, which in turn affects MG activation

The underlying mechanisms contributing to altered mitochondrial function, accompanied by elevated levels of ROS and lipid accumulation associated with hypersuccinylation, remain poorly understood. To elucidate whether the altered function was caused by changes in the expression levels of associated proteins in mitochondria, WB was used to assess the expression of proteins associated with the electron transport chain(ETC, Complex III and V), tricarboxylic acid(TCA) cycle(SDHA, which is one subunit of SDH enzyme) and lipid β-oxidation(ECHA). Surprisingly, no alterations in protein expression levels were observed in the Sirt5 KD cells compared to control cells, even upon treatment with LPS (Fig. 4A and S2E). These results suggest that the observed alterations in mitochondria function and lipid accumulation are unlikely to be a result of changes in the protein expression. The amount of mitochondria in both control and Sirt5 KD cells was further examined using Mito Red tracker staining and detected by FC. However, the MFI of Mito Red tracker did not show significant changes between control and Sirt5 KD cells, regardless of whether they were treated with LPS. This indicates that the quantity of mitochondria was not affected in the Sirt5 KD cells(Fig. 4B).

SDHA is one of the subunits comprising the SDH complex, which plays a crucial role in both ETC and the TCA cycle(Fig. 4D). Recent investigations have elucidated the pivotal role of SDH in ROS generation, thereby contributing to the initiation and progression of neurodegenerative diseases [45]. Considering the existing literature indicating the presence of multiple Lys succinylation sites on SDHA [46, 47], IP was conducted to isolate SDHA from control and Sirt5 KD BV2 cells for assessing its succinylation level. The result showed significantly higher level of succinylation on SDHA in Sirt5 KD cells compared to control cells(Fig. 4E). However, no disparity in SDH activity was observed between Sirt5 KD cells and control cells; nevertheless, it exhibited a significant increase following LPS treatment when compared to the untreated group(Fig. 4Fa). To mimic the insufficient energy supply during aging, an in vitro starvation model of BV2 cells was carried out(Fig. 4Ca). To our surprise, both control and Sirt5 KD cells exhibited significantly increased in SDH activity(Fig. 4Fb). These findings suggest that succinylation levels are associated with elevated SDH activity.

To validate the previously reported succinylated lysine residues(K250, K498, and K547) of SDHA, we transfected BV2 cells with Flag-tagged mutant forms SDHA(Fig. 4Cb). In these mutants, lysine was substituted by arginine to mimic the desuccinylated state(K-to-R mutants), or by glutamate to simulate the negatively charged succinylation modification(K-to-E mutants). Flag-tagged WT SDHA was used as the control for subsequent analysis of enzymatic activity(Fig. 4Cb). We found that all the K-to-E mutants cells exhibited significant increase in SDH activity(Fig. 4Fc). However, among K-to-R mutants, both K547R and K498R demonstrated varying increase in SDH activity except for K250R which displayed unaltered activity compared to control(Fig. 4Fc). These findings suggest that succinylation enhances enzymatic activity of SDH and Lys250 may serve as a critical lysine residue for succinylation. Furthermore, we investigated the mRNA expression of IL-6 in BV2 cells following introduction of the K-to-R or K-to-E mutant. Among the K-to-R mutants, only K498R exhibited higher level of IL-6 mRNA expression in LPS-treated mutant cells compared to untreated mutant cells(Fig. 4Ha). However, all K-to-E mutant cells exhibited significantly elevated IL-6 mRNA expression after LPS treatment(Fig. 4Hb). These results suggest that succinylation modification primarily regulates the enzymatic activity of SDH, subsequently influencing pro-inflammatory cytokine expression.

The metabolomic findings in this study revealed an enrichment of long chain lipids, indicating a reduction in lipid degradation. Therefore, we focused on ECHA, which is known to possess the 2,3-enoyl-CoA hydratase and the 3-hydroxyacyl-CoA dehydrogenase activities and is considered as the limiting factor for β-oxidation(Fig. 4I). ECHA has been reported to have the highest number of succinylation sites(28 sites) [48]. Consequently, we immunoprecipitated ECHA from control and Sirt5 KD BV2 cells for subsequent analysis of succinylation levels. We found a significant increase in the

succinylation level of ECHA(Fig. 4J), while the enzyme activity just exhibited slightly reduction in the Sirt5 KD cells compared to control cells(Fig. 4Ka). However, following LPS treatment, both control and Sirt5 KD cells exhibited a substantial decrease in enzyme activity, with the lowest activity observed in Sirt5 KD cells(Fig. 4Ka). Furthermore, we examined the impact of starvation on ECHA activity in both control and Sirt5 KD cells, revealing a significant reduction in ECHA activity. Notably, the activity was found to be decreased by half in the Sirt5 KD cells compared to the control group(Fig. 4Kb). These findings suggest that succinylation levels increase while there is a concurrent decrease in ECHA's enzymatic activity.

The succinylation modification of Lys 351, which is reported to be regulated by Sirt5, plays a crucial role in maintaining ECHA activity [29]. Therefore, BV2 cells were transfected with K-to-R or K-to-E mutants of K351, followed by enzymatic activity assays. The results showed that cells carrying K351E mutation, not the K351R mutation, exhibited a significant reduction(nearly 50%) in ECHA activity compared to control cells(Fig. 4Kc). Meanwhile, both K351E and K351R mutant exhibited significantly increased in IL-6 mRNA expression compared to control cells(Fig. 4L). However, only K351E mutant cells displayed a significant increase in IL-6 mRNA expression after undergoing LPS treatment compared to untreated cells(Fig. 4L). Collectively, these findings suggest that the succinylation modifications of SDHA and ECHA regulate the enzymes activities and affect the activated status of MGs.

The administration of SP effectively reverses aging-related phenotype of MGs by reducing the level of succinylation

Succinylation modification is primarily a spontaneous reaction wherein SCoA supplies the modified group, depending on the cellular or mitochondrial concentration of SCoA [25]. Hence, we investigated the possibility of modulating intracellular succinylation modifications by reducing SCoA level. SCoA serves as a crucial intermediate in the TCA cycle and is synthesized from α-ketoglutarate(α-KG) via α-ketoglutarate dehydrogenase complex(KGDHC) through decarboxylation(EC 1.2.4.2). Previous studies have reported that SP can inhibit KGDHC and reduce ROS production in the rat brain and cultured neurons (Fig. 5Aa) [49, 50]. Therefore, we employed SP as a KGDHC inhibitor to suppress SCoA production and downregulate succinylation levels. As illustrated in Fig. 5Ab, BV2 cells were pretreated with SP(10 μM)followed by LPS(100 ng/mL) treatment, then the succinylation level of mitochondrial proteins was analyzed using WB. The results showed that succinylation level was significantly reduced in SP pretreated cells compared to LPS treated alone(Fig. 5B). Meanwhile, the concentration of SCoA was also reduced(Fig. 5C), indicating SP pretreatment can significantly reduce the succinylation level by decreasing the concentration of SCoA in BV2 cells. Furthermore, MitoSox and NR staining were carried out again to analyze the generation of mtROS and the accumulation of lipids, as shown in Fig. 5D(Fig. 5D). The control and Sirt5 KD cells were stained with MitoSox or NR, followed by fluorescence microscopy (Fig. 5Ea and Fa) and FC analysis(Fig. 5Eb and Fb). Interestingly, pretreatment with SP alone led to a modest reduction in both the generation of mtROS and the accumulation of lipid droplets. However, when subjected to LPS treatment, a significant reduction in mtROS and lipid accumulation was observed in cells pretreated with SP(Fig. 5E, F). Additionally, the level of lipid peroxidation was also reduced in SP pretreated cells(Fig. 5G).

The expression levels of inflammatory cytokines, including *Il-1β*, *Tnf-α*, and *Il-6* were quantified using qPCR in SP pretreated PriMGs and BV2 cells with or without LPS treatment(Fig. 5D). The results showed that there were no significant differences between control and SP pretreated BV2 cells without LPS treatment(Fig. 5Hb). However, upon LPS treatment, except for *Il-1β*, both *Tnf-α*, and *Il-6* expression exhibited a significant reduction in SP pretreated cells compared to those treated with LPS alone in PriMGs(Fig. 5Ha). Similar findings were also observed in BV2 cells(Fig. 5Hb). In summary, these results suggest that administration of SP could attenuate the succinylation level by inhibiting the production of SCoA, thereby reducing ROS production, lipid accumulation and the inflammatory activation of MGs.

Subsequently, we investigated the potential of SP to ameliorate cellular senescence in BV2 cells. We established an in vitro aging model by treating BV2 cells with VP-16(Fig. 5I). Surprisingly, after 72 h of SP treatment, there was a significant reduction in the number of SA-β-Gal positive cells compared to VP-16 treatment alone(Fig. 5J). Furthermore, the effects of SP on desuccinylation were further validated in vivo using LPS ip. injection model(Fig. 5K). The hippocampal mitochondrial protein exhibited significantly up regulation of succinylation 24 h following LPS injection(Fig. 5L). Remarkably, pretreatment with SP reversed the level of succinylation and restored it close to that observed in control mice(Fig. 5L). Furthermore, IP was used to isolate SDHA and ECHA from the mouse hippocampus, and the succinylation level was measured by WB. It was interesting that, the succinylation level of SDHA and ECHA in the mice hippocampus was significantly increased after the LPS treatment. And was significantly reduced followed by the SP icv. treatment (Fig. S2F).

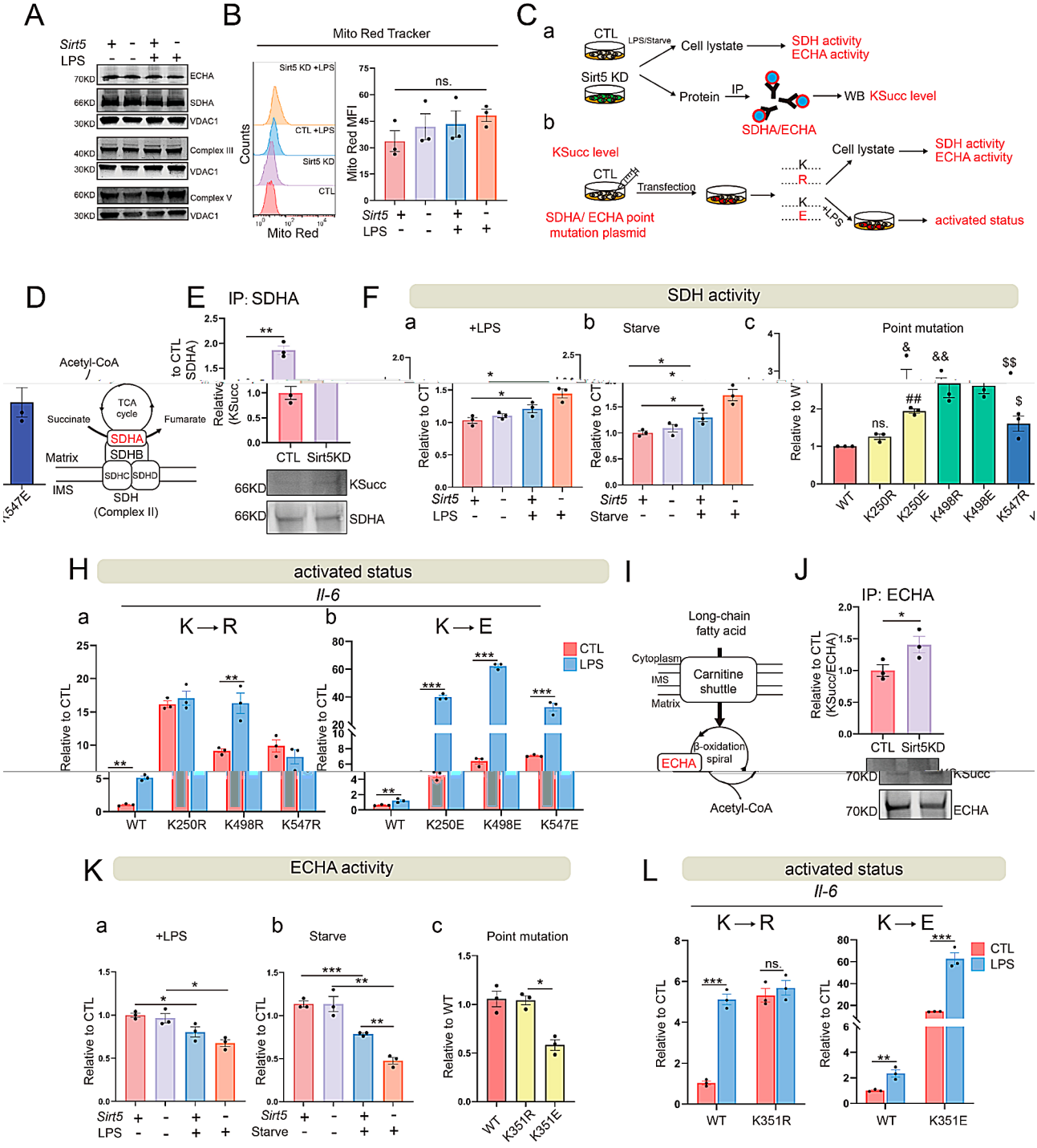

Fig. 4 Succinylation modification regulates SDH and ECHA activity, impacting MG activation. **(A)** WB analysis of mitochondrial proteins associated with β-oxidation(ECHA), TCA cycle(SDHA), ETC(Complex III and V). **(B)** The number of mitochondria stained with Mito red tracker and detected by FC. **(C)** Schematic experimental workflow; **(a)** Schematic of detecting SDH and ECHA activity detection and the succinylation level of SDHA and ECHA; **(b)** Schematic of succinyl sites point mutation and further experiments. **D.** Illustration of the role of SDH in the TCA cycle and ETC. **E.** WB analysis of succinylation level of SDHA following the IP. **F.** SDH enzyme activity analysis; **(a)** The enzyme activity of SDH under the inflamed (+LPS); **(b)** energy shortage (Starve) situation in the BV2 cells; **(c)** The enzyme activity of SDH following the point mutation of K250, K498 and K547 in the BV2 cells. K250E vs. WT ## $P < 0.01$, &(K498R vs. WT) $P < 0.05$, &&(K498E vs. WT) $P < 0.01$, $(K547R vs. WT) $P < 0.05$, $$(K547E vs. WT) $P < 0.01$. **H.** Pro-inflammatory cytokines transcription level of *Il-6* under inflamed condition detected by qPCR following the point mutation of K250, K498 and K547 in the BV2 cells. **I.** Illustration of the central role of ECHA in the lipid β-oxidation. **J.** WB analysis of succinylation level of ECHA following the IP. **K.** ECHA enzyme activity analysis; **(a)** The enzyme activity of ECHA under the inflamed (+LPS); **(b)** energy shortage (Starve) situation in the BV2 cells; **(c)** The enzyme activity of ECHA following the point mutation of K351 in the BV2 cells. **L.** Proinflammatory cytokines transcription level of *Il-6* under inflamed condition detected by qPCR following the point mutation of K351 in the BV2 cells. $n = 3$/group, * $P < 0.05$, ** $P < 0.01$, *** $P < 0.005$, **** $P < 0.001$

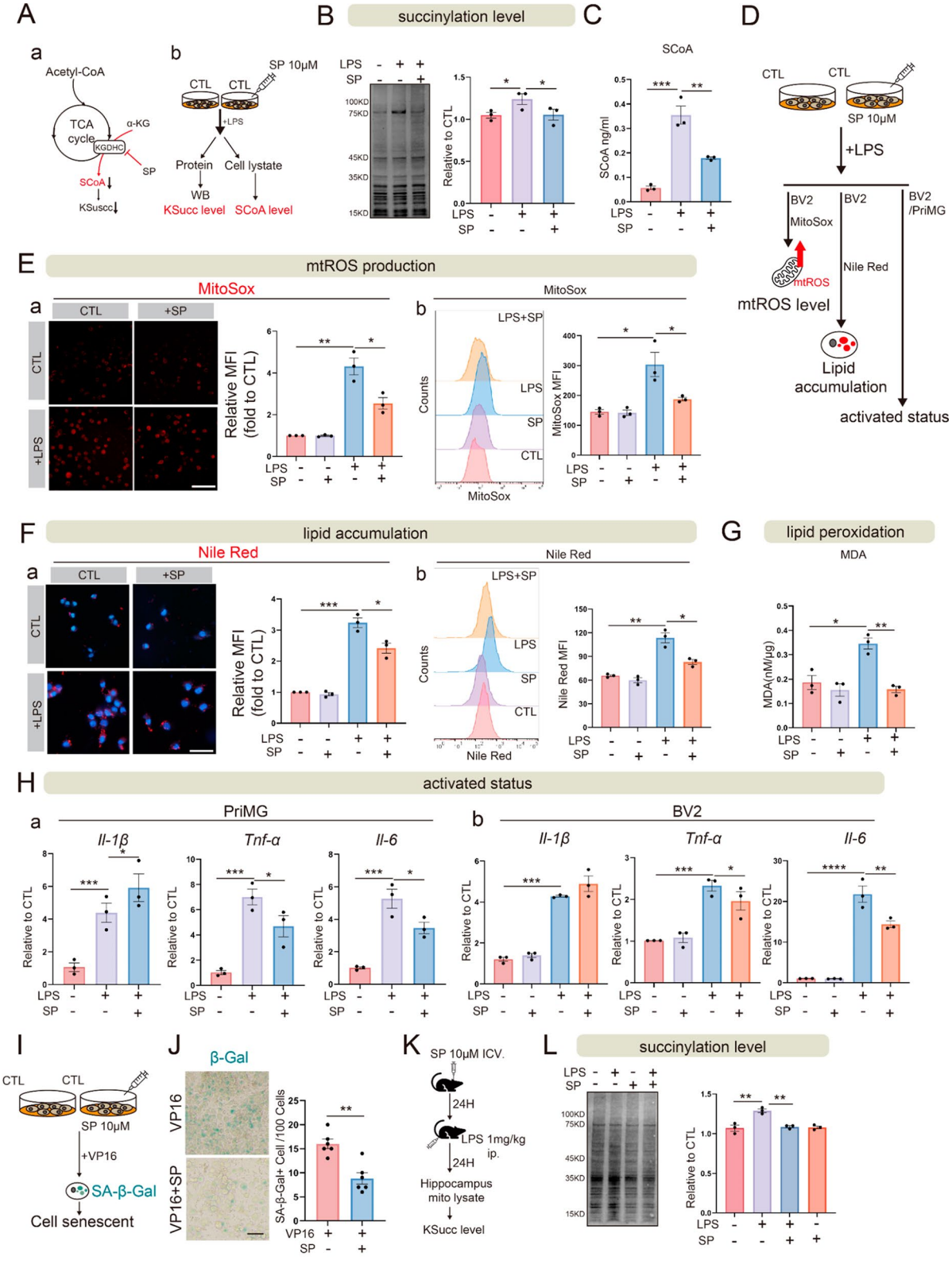

Fig. 5 (See legend on next page.)

(See figure on previous page.)

Fig. 5 SP administration reverses MGs' aging phenotype by reducing the level of succinylation. **A.** Schematic illustration of **(a)** the generation of SCoA via KGDHC and the metabolite changes follow the SP treatment, **(b)** Schematic workflow of the experiment of SP pretreatment and the following experiments. **B.** Succinylation level of LPS treatment with or without SP pretreatment in BV2 cells were detected by WB. **C.** The concentration of SCoA in cellular total lysate of LPS treatment with or without SP pretreatment in BV2 cells were detected by colorimetric method. **D.** Schematic workflow of detecting the senescence MG indicators after SP pretreatment. **E.** mtROS generation was detected by MitoSox staining after the SP pretreatment in the physiological and inflammatory condition; **(a)** mtROS generation was observed and detected by fluorescence microscopy and the MFI was measured. Bar = 50 μm; **(b)** mtROS generation of BV2 cells treated with SP and LPS was detected by FC. **F.** Lipid accumulation was detected by Nile Red staining after the SP pretreatment in the physiological and inflammatory condition; **(a)** Lipid accumulation was observed and detected by fluorescence microscopy and the MFI was measured. Bar = 50 μm; **(b)** Lipid accumulation of BV2 cells treated with SP and LPS was detected by FC. **G.** MDA concentration of BV2 cells treated with SP and LPS was detected by colorimetric method. **H.** Pro-inflammatory cytokines transcription level of *Il-1β*, *Il-6* and *Tnf-α* in the, **(a)** PriMGs and **(b)** BV2 cells treated with SP and LPS were detected by qPCR. **I.** Schematic workflow of SP pretreatment in the VP16 induced aging model. **J.** SA-β-Gal positive cells were counted and calculated following the pretreatment of SP in the VP16 induced aging model. Bar = 50 μm **K.** Schematic workflow of SP pretreatment in the in vivo neuroinflammation model. **L.** The succinylation level of the hippocampus mito lysate of the in vivo neuroinflammation model pretreated with SP was detected by WB. $n = 3$/group, * $P < 0.05$, ** $P < 0.01$, *** $P < 0.005$, **** $P < 0.001$

Discussion

In the present study, we have discovered the relationship between succinylation modification and CNS aging. Our findings indicate that succinylation levels are increased in aged mouse brains and MGs. In vitro experiments demonstrate that upregulated succinylation results in metabolic reprogramming with weakened mitochondrial adaptability and enhanced glycolysis. Meanwhile, under inflammatory conditions, upregulated succinylation leads to dramatic heightened cell reactivity with increased mtROS production and lipid accumulation. Furthermore, the metabolomics analysis reveals those significant alterations in various metabolites due to upregulated succinylation, particularly affecting lipids and lipid-like molecules. The up-regulated metabolites mostly enriched in the glycolysis and related metabolic pathways while excluding OXPHOS, whereas down-regulated metabolites were mainly associated with FA metabolism. We hypothesize that these consequences may be related to the imbalanced activities of SDH and ECHA, which are regulated by succinylation. Finally, we demonstrate that reducing the SCoA production can decrease the succinylation level in vivo and in vitro, thereby alleviating the senescent state of MG. To our knowledge, our data provides evidence revealing succinylation modification as a potential link between MG energy metabolism and activation in CNS aging. These results offer further insight into the mechanism of aging-related neuroinflammation as well as interventions of CNS aging from a novel perspective.

Although limited studies have investigated the association between succinylation and CNS aging, existing evidence has substantiated an elevated level of succinylation modification in aging-related degenerative conditions such as ovarian aging, osteopenia, and disc herniation. These findings underscore a potential correlation between succinylation and the process of aging [26, 51, 52]. Succinylation exerts a significant influence on multiple cellular processes, including gene transcription, energy metabolism, protein folding and translocation [53–55]. Among these processes, the important role of succinylation in metabolic processes has been extensively documented. Notably, succinylation profoundly impacts energy metabolism by predominantly occurring within mitochondria and modulating enzymes involved in this process. Under physiological conditions, these enzymes maintain a delicate balance of succinylation and desuccinylation [28]. However, during aging, the balance is disrupted leading to a state of hypersuccinylation that may perturb the mitochondrial energy metabolism and subsequently result in cellular dysfunction across various organs. The brain is the most metabolically active organ, and succinylation has been reported as a pivotal factor contributing to CNS diseases, including ischemic/hemorrhagic stroke and neurodegenerative diseases, which are associated with inadequate energy supply in the CNS and aberrant energy metabolism in the neurons [56–59]. Our findings suggest that the impaired energy metabolism may be greatly due to the functional impacts of upregulated succinylation of key enzymes in the mitochondria. Moreover, succinylation modification is highly sensitive to metabolic changes, as SCoA, the donor of succinyl group, is an intermediate metabolite in the TCA cycle and consistently fluctuates with changes in metabolic levels [28]. Metabolic perturbations of CNS, such as cerebral ischemia, low metabolic levels during depression and aging-related reduction of metabolism can alter succinylation of mitochondrial proteins [60–62]. Therefore, succinylation serves as a valuable indicator for altered energy metabolism related to aging that involves interactions between succinylated proteins and metabolic challenges.

It is crucial to emphasize that PTMs do not occur in isolation, as proteins undergo diverse modifications at different residues and types. From the omics data on protein modification reveals intricate crosstalk between succinylation and other modifications, particularly acetylation. In our findings, a significant increase in SDH activity was observed following the point mutation of SDHA at K498R, which is intended to mimic the desuccinylated state. It has been previously reported that K498 can undergo modifications such as succinylation and

acetylation, with acetylation on K498 leading to downregulation of SDH activity [63]. The point mutation of K498R also abolishes the inhibitory effect of acetylation on SDH activity.

The balance between succinylation and desuccinylation is regulated by the levels or the activities of modification writers and the erasers [28]. Succinylation has been reported to occur spontaneously, which correlates with the concentration of SCoA in the mitochondria. In contrast, Sirt5 is currently the only known desuccinylase found in all cell compartments, predominantly localized within mitochondria [29]. The sirtuins, a family of NAD^+ dependent lysine deacetylases, are involved in a variety of physiological processes related to aging, including oxidative stress, apoptosis and inflammation [64, 65]. Recent study has demonstrated that deficiency in any sirtuin leads to accelerated cellular senescence [66]. In our study, we observed a significant upregulation of aging and DAM-related genes expressions, accompanied by an elevated level of mitochondrial succinylation following Sirt5 KD. These data suggest that the important role of Sirt5 in modulating the aging process through its regulation of succinylation level. Under physiological conditions, Sirt5 is activated in response to energy deprivation and facilitates desuccinylation of metabolic enzymes within the mitochondria, thereby functioning as a metabolic level sensor [67]. However, under conditions such as aging or other pathological states that disrupt the balance between succinylation and desuccinylation, dysfunction of metabolic enzymes occur, resulting in accelerated aging and neurodegeneration diseases.

The majority of research on succinylation modification in the CNS primarily focuses on its impact on neurons, with only a limited number of studies investigating MG [57, 68]. As the principal immune cell in the brain, MG possesses the remarkable ability to dynamically regulate nutrient uptake and metabolic enzyme activity, enabling them to adapt to the intricate and dynamic microenvironment of the brain. This phenomenon is commonly referred to as metabolic reprogramming [11, 69], which empowers MGs to effectively execute their essential immune surveillance function. It is well known that MG primarily utilizes OXPHOS and FA oxidation as the predominant metabolic pathway in the resting state but undergoes a metabolic shift towards glycolysis during the pro-inflammatory status. This metabolic reprogramming is orchestrated by transcriptional upregulation of specific genes and altered activities of key metabolic enzymes [12]. Succinylation has been reported to regulate the activities of enzymes in major metabolic pathways including TCA cycle, glycolysis, FA oxidation, urea cycle, and nucleotide metabolism [45]. This finding was further supported by our metabolomics study, which employed KEGG enrichment analysis and differential metabolite identification. SDHA, the subunit of SDH, which is also known as complex II on the mitochondrial ETC, was previously reported to be modified by succinylation and regulated by Sirt5 [46]. In our study, we found the succinylation level of SDHA was increased after the Sirt5 KD, confirming that Sirt5 regulates the succinylation level in MG. We further confirmed that succinylation modification of Lys 250 can regulate SDH activity and influence the release of pro-inflammatory cytokines in MG. SDH plays a crucial role in coupling two major energy metabolism pathways within mitochondria, namely the TCA cycle and the oxidative respiratory chain, both essential for mitochondrial OXPHOS [70]. In the context of ischemia/reperfusion (I/R), ETC is widely acknowledged as the primary source of ROS. The elevation in ROS levels during I/R predominantly stems from SDH, which induces a reversed electron transfer(RET) at complex I, thereby triggering an upsurge in ROS generation and exacerbating cerebral I/R injury [45, 71]. In this study, the succinylation of SDHA positively regulates the activity of SDH enzyme, and a significant increase in mtROS level was observed with an increase succinylation level. We propose that the elevation in mtROS level is associated with overactivation of SDH induced by increased succinylation modification of SDHA.

Lipid drops accumulation is reported as a key feature of MG activation [8, 72]. In our study, we found an increase in the number of intracellular lipid droplets in Sirt5 KD cells, which correlated with elevated transcription levels of aging and DAM-related genes. It has been reported that ECHA, a key rate-limiting enzyme responsible for the β-oxidation of intracellular FAs, is regulated by Sirt5 induced desuccinylation [48, 73]. Therefore, we hypothesized that lipid accumulation after Sirt5 KD is related to the retardation of FAs β-oxidative due to downregulation of ECHA enzyme activity. In summary, the elevated succinylation levels of SDHA and ECHA disrupt the balance between TCA cycle, ETCs and the lipid β-oxidation, resulting in increased ROS production, lipid accumulation and lipid peroxidation. These consequences may contribute to the metabolic reprogramming and dystrophy in aging MGs.

Sirt5, being the sole regulator of desuccinylation, has been extensively investigated in the context of anti-aging processes. Resveratrol, abundantly present in fruits and commonly consumed foods, has been reported to modulate Sirt5 activity and effectively reduce succinylation levels [74, 75]. However, its efficacy requires administration of high doses, and its limited water solubility hampers widespread application. Moreover, the function of Sirt5 is inconsistent across different diseases such as ischemic stroke [76], in which the increasing expression of Sirt5 has been found to promote disease progression. This makes us cautious about blindly increasing Sirt5

activity by sirtuin activators. Succinylation mainly occurs predominantly through non-enzymatic mechanisms, which depend on the concentration of SCoA. In our study, we employed SP to inhibit KGDHC activity and consequently impede SCoA production. Pre-treatment with SP in the inflammatory state resulted in a reduction in succinylation levels, leading to decreased ROS production, lipid accumulation, and MG activation. Furthermore, SP pre-treatment significantly diminished the number of senescent MG cells in an in vitro aging model. In vivo experiments demonstrated that hippocampal succinylation levels were reduced by SP pre-treatment in a neuroinflammation model. In our data, we also observed the diversity in the regulatory mechanisms of metabolic pathways on MG reactivity. For instance, SP significantly reduced the mRNA level of IL-6 and TNF-α in BV2 cells, except for IL-1β. Previous studies have reported that mitochondrial metabolites regulate macrophage inflammatory responsiveness through two distinct pathways: one involving succinic acid or SCoA regulated by IL-6, and another bypass pathway mediated by glutamine [77]. To further investigate whether the IL-1β production pathway in MG is also regulated by the replenishment effect of glutamine, we cultured cells with glutamine-free medium and administered SP treatment. We observed that in the absence of glutamine, SP inhibited the mRNA level of IL-1β. Indeed, a long-term SP intervention should be carried out in aged mice to evaluate the anti-aging ability of SP in vivo, that will be our next task.

Conclusions

In summary, our data demonstrates the relationship between succinylation modification and the aging-related neuroinflammation. By regulating the level of succinylation, we could modulate the metabolic mode and manipulate the cell reactivity, ultimately alleviating MG senescence. Our findings will provide further insight into the treatment of aging-related neuroinflammation.

Abbreviations

AD	Alzheimer's disease
ATP	Aadenosine triphosphate
CNS	Central nervous system
DAM	Disease-associated microglia
ECAR	Extracellular acidification rate
ECHA	Trifunctional enzyme subunit alpha
ETC	Electron transport chain
FACS	Fluorescence-activated cell sorting
ICV	Intracerebroventricular
IHC	Immunohistochemistry
ip.	Intraperitoneal injection
KGDHC	α-ketoglutarate dehydrogenase complex
LA	Lactic acid
LDAM	Lipid-droplet-accumulating microglia
LPS	Lipopolysaccharide
MDA	Malondialdehyde
MFI	Mean fluorescent intensity
MG	Microglia
OCR	Oxygen consumption rate
OPLS-DA	Orthogonal partial least-squares discriminant analysis
OXPHOS	Oxidative phosphorylation
PD	Parkinson's disease
PER	Proton efflux rate
PFA	Paraformaldehyde
PTM	Post-translational modification
ROS	Reactive oxygen species
SASP	Senescence-associated secretory phenotype
SCoA	Succinyl-CoA
SDH	Succinate dehydrogenase
Sirt5 KD	Sirt5-knockdown
SP	Succinyl phosphonate
TCA	Tricarboxylic acid
WB	Western blot
α-KG	α-ketoglutarate

Supplementary Information

The online version contains supplementary material available at https://doi.org/10.1186/s12974-024-03284-4.

Supplementary Material 1

Supplementary Material 2

Supplementary Material 3

Supplementary Material 4

Acknowledgements

We are grateful to Shanghai Applied Protein Technology Co., Ltd., China, for their help in processing the untargeted metabolomics. We sincerely thank Mei Li and Lingling Jin for their invaluable support and assistance with the Seahorse experiments.

Author contributions

X.Z., K.F. and J.M. wrote the main manuscript text. X.Z. and X. Y. prepared the Figs. 1 and 2. C. D. and S.L. prepared the primary cells culture and flow-cytometry analysis. H.H. , G.Z. and G.L. prepared the Figs. 3, 4 and 5. All authors reviewed the manuscript.

Funding

Dalian Medical University Interdisciplinary Research Cooperation Project Team Funding JCHZ2023007.

Data availability

No datasets were generated or analysed during the current study.

Declarations

Ethical approval

All procedures were in accordance with the Dalian Medical University guidelines for the proper care and use of laboratory animals and were approved by the Laboratory Animal Care and Use Committee of Dalian Medical University.

Consent for publication

Not applicable.

Competing interests

The authors declare no competing interests.

Author details

[1]Department of Anatomy, College of Basic Medical Sciences, Dalian Medical University, Dalian, Liaoning, China
[2]Department of Morphology, College of Basic Medical Sciences, Dalian Medical University, Dalian, Liaoning, China
[3]National-Local Joint Engineering Research Center for Drug-Research and Development (R&D) of Neurodegenerative Diseases, Dalian Medical University, Dalian, Liaoning, China

Received: 23 July 2024 / Accepted: 1 November 2024
Published online: 14 November 2024

References

1. Erkkinen MG, Kim MO, Geschwind MD. Clinical neurology and epidemiology of the Major Neurodegenerative diseases. Cold Spring Harb Perspect Biol. 2018;10(4):a033118.
2. Kwon HS, Koh SH. Neuroinflammation in neurodegenerative disorders: the roles of microglia and astrocytes. Transl Neurodegener. 2020;9(1):42.
3. Marogianni C, Sokratous M, Dardiotis E, Hadjigeorgiou GM, Bogdanos D, Xiromerisiou G. Neurodegeneration and Inflammation-An interesting interplay in Parkinson's Disease. Int J Mol Sci. 2020;21(22):8421.
4. Colonna M, Butovsky O. Microglia function in the Central Nervous System during Health and Neurodegeneration. Annu Rev Immunol. 2017;35:441–68.
5. Zhang S, Meng R, Jiang M, Qing H, Ni J. Emerging roles of Microglia in Blood-Brain Barrier Integrity in Aging and Neurodegeneration. Curr Neuropharmacol. 2024;22(7):1189–204.
6. Elyahu Y, Hekselman I, Eizenberg-Magar I, et al. Aging promotes reorganization of the CD4 T cell landscape toward extreme regulatory and effector phenotypes. Sci Adv. 2019;5(8):eaaw8330.
7. Kaya T, Mattugini N, Liu L, et al. CD8 + T cells induce interferon-responsive oligodendrocytes and microglia in white matter aging. Nat Neurosci. 2022;25(11):1446–57.
8. Marschallinger J, Iram T, Zardeneta M et al. Lipid-droplet-accumulating microglia represent a dysfunctional and proinflammatory state in the aging brain [published correction appears in Nat Neurosci. 2020;23(2):294. https://doi.org/10.1038/s41593-020-0595-9] [published correction appears in Nat Neurosci. 2020;23(10):1308.
9. Silvin A, Uderhardt S, Piot C, et al. Dual ontogeny of disease-associated microglia and disease inflammatory macrophages in aging and neurodegeneration. Immunity. 2022;55(8):1448–e14656.
10. Deczkowska A, Keren-Shaul H, Weiner A, Colonna M, Schwartz M, Amit I. Disease-Associated Microglia: a Universal Immune Sensor of Neurodegeneration. Cell. 2018;173(5):1073–81.
11. Sabogal-Guáqueta AM, Marmolejo-Garza A, Trombetta-Lima M, et al. Species-specific metabolic reprogramming in human and mouse microglia during inflammatory pathway induction. Nat Commun. 2023;14(1):6454.
12. Orihuela R, McPherson CA, Harry GJ. Microglial M1/M2 polarization and metabolic states. Br J Pharmacol. 2016;173(4):649–65.
13. Monsorno K, Buckinx A, Paolicelli RC. Microglial metabolic flexibility: emerging roles for lactate. Trends Endocrinol Metab. 2022;33(3):186–95.
14. Joshi L, Plastira I, Bernhart E, et al. Lysophosphatidic acid induces aerobic glycolysis, Lipogenesis, and increased amino acid uptake in BV-2 microglia. Int J Mol Sci. 2021;22(4):1968.
15. Pan RY, He L, Zhang J, et al. Positive feedback regulation of microglial glucose metabolism by histone H4 lysine 12 lactylation in Alzheimer's disease. Cell Metab. 2022;34(4):634–e6486.
16. Huang ZP, Liu SF, Zhuang JL, et al. Role of microglial metabolic reprogramming in Parkinson's disease. Biochem Pharmacol. 2023;213:115619.
17. Cherry JD, Olschowka JA, O'Banion MK. Neuroinflammation and M2 microglia: the good, the bad, and the inflamed. J Neuroinflammation. 2014;11:98.
18. Yang S, Qin C, Hu ZW, et al. Microglia reprogram metabolic profiles for phenotype and function changes in central nervous system. Neurobiol Dis. 2021;152:105290.
19. Lee JM, Hammarén HM, Savitski MM, Baek SH. Control of protein stability by post-translational modifications. Nat Commun. 2023;14(1):201.
20. Zou L, Yang Y, Wang Z, et al. Lysine Malonylation and its links to Metabolism and diseases. Aging Dis. 2023;14(1):84–98.
21. Zhang Z, Tan M, Xie Z, Dai L, Chen Y, Zhao Y. Identification of lysine succinylation as a new post-translational modification. Nat Chem Biol. 2011;7(1):58–63.
22. Xie L, Xiao Y, Meng F, Li Y, Shi Z, Qian K. Functions and mechanisms of lysine glutarylation in eukaryotes. Front Cell Dev Biol. 2021;9:667684.
23. Das T, Yount JS, Hang HC. Protein S-palmitoylation in immunity. Open Biol. 2021;11(3):200411.
24. Diskin C, Ryan TAJ, O'Neill LAJ. Modification of proteins by metabolites in Immunity. Immunity. 2021;54(1):19–31.
25. Lancaster MS, Kim B, Doud EH, et al. Loss of succinyl-CoA synthetase in mouse forebrain results in hypersuccinylation with perturbed neuronal transcription and metabolism. Cell Rep. 2023;42(10):113241.
26. Le M, Li J, Zhang D, et al. The emerging role of lysine succinylation in ovarian aging. Reprod Biol Endocrinol. 2023;21(1):38.
27. Zhang LL, Li CW, Liu K, et al. Discovery and Identification of serum succinyl-proteome for postmenopausal women with osteoporosis and Osteopenia. Orthop Surg. 2019;11(5):784–93.
28. Yang Y, Gibson GE. Succinylation Links metabolism to protein functions. Neurochem Res. 2019;44(10):2346–59.
29. Du J, Zhou Y, Su X, et al. Sirt5 is a NAD-dependent protein lysine demalonylase and desuccinylase. Science. 2011;334(6057):806–9.
30. Zhao X, Liu G, Yu X, et al. Ablation of AQP5 gene in mice leads to olfactory dysfunction caused by hyposecretion of Bowman's gland. Chem Senses. 2023;48:bjad030.
31. Sadhukhan S, Liu X, Ryu D, et al. Metabolomics-assisted proteomics identifies succinylation and SIRT5 as important regulators of cardiac function. Proc Natl Acad Sci U S A. 2016;113(16):4320–5.
32. Caldeira C, Oliveira AF, Cunha C, et al. Microglia change from a reactive to an age-like phenotype with the time in culture. Front Cell Neurosci. 2014;8:152.
33. Rim C, You MJ, Nahm M, Kwon MS. Emerging role of senescent microglia in brain aging-related neurodegenerative diseases. Transl Neurodegener. 2024;13(1):10.
34. Li X, Li Y, Jin Y, et al. Transcriptional and epigenetic decoding of the microglial aging process. Nat Aging. 2023;3(10):1288–311.
35. Wang B, Han J, Elisseeff JH, Demaria M. The senescence-associated secretory phenotype and its physiological and pathological implications. Nat Rev Mol Cell Biol. 2024.
36. Koellhoffer EC, McCullough LD, Ritzel RM. Old maids: Aging and its impact on Microglia function. Int J Mol Sci. 2017;18(4):769.
37. Wagner GR, Payne RM. Widespread and enzyme-independent Nε-acetylation and Nε-succinylation of proteins in the chemical conditions of the mitochondrial matrix. J Biol Chem. 2013;288(40):29036–45.
38. Zhu L, Zhao Q, Yang T, Ding W, Zhao Y. Cellular metabolism and macrophage functional polarization. Int Rev Immunol. 2015;34(1):82–100.
39. Singh A, Schurman SH, Bektas A, et al. Aging and inflammation. Cold Spring Harb Perspect Med. 2024;14(6):a041197.
40. Triviño JJ, von Bernhardi R. The effect of aged microglia on synaptic impairment and its relevance in neurodegenerative diseases. Neurochem Int. 2021;144:104982.
41. Simpson DSA, Oliver PL. ROS Generation in Microglia: understanding oxidative stress and inflammation in neurodegenerative disease. Antioxid (Basel). 2020;9(8):743.
42. Mas-Bargues C, Escrivá C, Dromant M, Borrás C, Viña J. Lipid peroxidation as measured by chromatographic determination of malondialdehyde. Human plasma reference values in health and disease. Arch Biochem Biophys. 2021;709:108941.
43. Dham D, Roy B, Gowda A, et al. 4-Hydroxy-2-nonenal, a lipid peroxidation product, as a biomarker in diabetes and its complications: challenges and opportunities. Free Radic Res. 2021;55(5):547–61.
44. Yan LJ. Positive oxidative stress in aging and aging-related disease tolerance. Redox Biol. 2014;2:165–9.
45. Mills EL, Kelly B, Logan A, et al. Succinate dehydrogenase supports metabolic repurposing of Mitochondria to Drive Inflammatory macrophages. Cell. 2016;167(2):457–e47013.
46. Park J, Chen Y, Tishkoff DX, et al. SIRT5-mediated lysine desuccinylation impacts diverse metabolic pathways. Mol Cell. 2013;50(6):919–30.
47. Liu Z, Wang R, Wang Y, Duan Y, Zhan H. Targeting succinylation-mediated metabolic reprogramming as a potential approach for cancer therapy. Biomed Pharmacother. 2023;168:115713.
48. Rardin MJ, He W, Nishida Y, et al. SIRT5 regulates the mitochondrial lysine succinylome and metabolic networks. Cell Metab. 2013;18(6):920–33.
49. Bunik VI, Denton TT, Xu H, Thompson CM, Cooper AJ, Gibson GE. Phosphonate analogues of alpha-ketoglutarate inhibit the activity of the alpha-ketoglutarate dehydrogenase complex isolated from brain and in cultured cells. Biochemistry. 2005;44(31):10552–61.
50. Artiukhov AV, Graf AV, Kazantsev AV, et al. Increasing inhibition of the rat brain 2-Oxoglutarate dehydrogenase decreases glutathione Redox State, elevating anxiety and perturbing stress adaptation. Pharmaceuticals (Basel). 2022;15(2):182.
51. Zhang LL, Li CW, Liu K, Liu Z, Liang BC, Yang YR, Shi XL. Discovery and Identification of serum succinyl-proteome for postmenopausal women with osteoporosis and Osteopenia. Orthop Surg. 2019;11(5):784–93.
52. Mao J, Wang D, Wang D, et al. SIRT5-related desuccinylation modification of AIFM1 protects against compression-induced intervertebral disc

degeneration by regulating mitochondrial homeostasis. Exp Mol Med. 2023;55(1):253–68.
53. Wang Y, Guo YR, Liu K, et al. KAT2A coupled with the α-KGDH complex acts as a histone H3 succinyltransferase. Nature. 2017;552(7684):273–7.
54. Zhang Y, Bharathi SS, Rardin MJ, et al. Lysine desuccinylase SIRT5 binds to cardiolipin and regulates the electron transport chain. J Biol Chem. 2017;292(24):10239–49.
55. Wang F, Wang K, Xu W, et al. SIRT5 desuccinylates and activates pyruvate kinase M2 to Block macrophage IL-1β production and to prevent DSS-Induced Colitis in mice. Cell Rep. 2017;19(11):2331–44.
56. Huang LY, Ma JY, Song JX, et al. Ischemic accumulation of succinate induces Cdc42 succinylation and inhibits neural stem cell proliferation after cerebral ischemia/reperfusion. Neural Regen Res. 2023;18(5):1040–5.
57. Xiao ZP, Lv T, Hou PP, et al. Sirtuin 5-Mediated lysine Desuccinylation protects mitochondrial metabolism following subarachnoid hemorrhage in mice. Stroke. 2021;52(12):4043–53.
58. Yang Y, Tapias V, Acosta D, et al. Altered succinylation of mitochondrial proteins, APP and tau in Alzheimer's disease. Nat Commun. 2022;13(1):159.
59. Qin Y, Yang P, He W, et al. Novel histone post-translational modifications in Alzheimer's disease: current advances and implications. Clin Epigenetics. 2024;16(1):39.
60. Shin TH, Lee DY, Basith S, et al. Metabolome changes in cerebral ischemia. Cells. 2020;9(7):1630.
61. Jiang M, Wang L, Sheng H. Mitochondria in depression: the dysfunction of mitochondrial energy metabolism and quality control systems. CNS Neurosci Ther. 2024;30(2):e14576.
62. Amorim JA, Coppotelli G, Rolo AP, Palmeira CM, Ross JM, Sinclair DA. Mitochondrial and metabolic dysfunction in ageing and age-related diseases. Nat Rev Endocrinol. 2022;18(4):243–58.
63. Cimen H, Han MJ, Yang Y, Tong Q, Koc H, Koc EC. Regulation of succinate dehydrogenase activity by SIRT3 in mammalian mitochondria. Biochemistry. 2010;49(2):304–11.
64. Ji Z, Liu GH, Qu J. Mitochondrial sirtuins, metabolism, and aging. J Genet Genomics. 2022;49(4):287–98.
65. Singh CK, Chhabra G, Ndiaye MA, Garcia-Peterson LM, Mack NJ, Ahmad N. The role of sirtuins in antioxidant and Redox Signaling. Antioxid Redox Signal. 2018;28(8):643–61.
66. Bi S, Jiang X, Ji Q, et al. The sirtuin-associated human senescence program converges on the activation of placenta-specific gene PAPPA. Dev Cell. 2024;59(8):991–e100912.
67. Nishida Y, Rardin MJ, Carrico C, et al. SIRT5 regulates both cytosolic and mitochondrial protein malonylation with Glycolysis as a major target. Mol Cell. 2015;59(2):321–32.
68. Gibson GE, Xu H, Chen HL, Chen W, Denton TT, Zhang S. Alpha-ketoglutarate dehydrogenase complex-dependent succinylation of proteins in neurons and neuronal cell lines. J Neurochem. 2015;134(1):86–96.
69. Hu Y, Mai W, Chen L, et al. mTOR-mediated metabolic reprogramming shapes distinct microglia functions in response to lipopolysaccharide and ATP. Glia. 2020;68(5):1031–45.
70. Jodeiri Farshbaf M, Kiani-Esfahani A. Succinate dehydrogenase: Prospect for neurodegenerative diseases. Mitochondrion. 2018;42:77–83.
71. Markevich NI, Markevich LN. Computational Modeling Analysis of Kinetics of Fumarate reductase activity and ROS production during reverse Electron transfer in mitochondrial respiratory complex II. Int J Mol Sci. 2023;24(9):8291.
72. Haney MS, Pálovics R, Munson CN, et al. APOE4/4 is linked to damaging lipid droplets in Alzheimer's disease microglia. Nature. 2024;628(8006):154–61.
73. Nakamura MT, Yudell BE, Loor JJ. Regulation of energy metabolism by long-chain fatty acids. Prog Lipid Res. 2014;53:124–44.
74. Zhou DD, Luo M, Huang SY, Saimaiti A, Shang A, Gan RY, Li HB. Effects and mechanisms of Resveratrol on Aging and Age-Related diseases. Oxid Med Cell Longev. 2021;2021:9932218.
75. Pyo IS, Yun S, Yoon YE, Choi JW, Lee SJ. Mechanisms of aging and the Preventive effects of Resveratrol on Age-Related diseases. Molecules. 2020;25(20):4649.
76. Xia Q, Gao S, Han T, et al. Sirtuin 5 aggravates microglia-induced neuroinflammation following ischaemic stroke by modulating the desuccinylation of Annexin-A1. J Neuroinflammation. 2022;19(1):301.
77. Tannahill GM, Curtis AM, Adamik J, et al. Succinate is an inflammatory signal that induces IL-1β through HIF-1α. Nature. 2013;496(7444):238–42.

Publisher's note